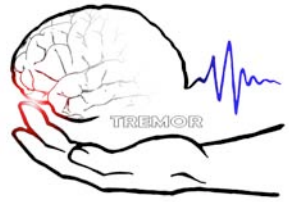

TREMOR. An ambulatory BCI-driven tremor suppression system based on functional electrical stimulation

Contract: FP7-ICT-2007-224051

Seventh Framework Programme, EU

BCI algorithms for tremor identification, characterization and tracking

Author(s): L. Barrios, J.A. Gallego, J. Ibañez, A.R. Vitoria, G. Severini, S. Conforto, T. D'Alessio, J.L. Dideriksen, F. Gianfelici, S. Dosen, D. Farina, J.O. Roa, E. Rocon, J.L. Pons
Partner(s): CSIC, URT, AAU, TCN
Workpackage: WP4
Date of preparation: 07.10.2011
Version number: v3.0

Table of contents

Executive summary

The TREMOR neurorobot comprises a Brain Neural Computer Interface that monitors the whole neuromusculoskeletal system, aiming at characterizing both voluntary movement and tremor, and a Functional Electrical Stimulation system that compensates for tremorous movements without impeding the user perform functional tasks. This document will describe the work developed in the framework of WP4 in order to extract both voluntary movement and tremor information, and deliver 1) the intention to perform voluntary movement, 2) tremor onset, and 3) tremor frequency and amplitude at each anatomical joint in a Real-Time, recursive and adaptive implementation. Preliminary experimental results are used to illustrate the performance of the different modalities of this BNCI interface.

Change history record

The overall content of this document has been kept with respect to the previous version (V2.0) approved in a previous review. The unique change of this new version is the inclusion of a study (included as Annex 2 to this document) carried out by the consortium in order to address recommendation 6 of the second review meeting:

> R6: The BCI prediction of voluntary movement has led to promising experimental results in the lab environment. However, precision and recall drastically change from one patient to another. The consortium is advised to investigate on which class of patients the method works best.

1. Introduction

The TREMOR neurorobot monitors the neuromusculoskeletal system to characterize both concomitant voluntary and tremorous movements based on a Brain Neural Computer Interface (BNCI), and then stimulates upper limb muscles to compensate functionally for the tremor. As all wearable robots, the major characteristic of the TREMOR neurorobot is its strong interaction with the user, [68]. This interaction is both physical and cognitive, and happens in a bidirectional manner. In our case, the cognitive Human–Robot Interface (cHRI) is built upon a BNCI that assesses the generation, transmission, and execution of both voluntary and tremorous movements. On the other hand, the physical Human–Robot Interface (pHRI) comprises a multichannel FES system that selectively drives the muscles based on the output of the control algorithm, Figure 1.

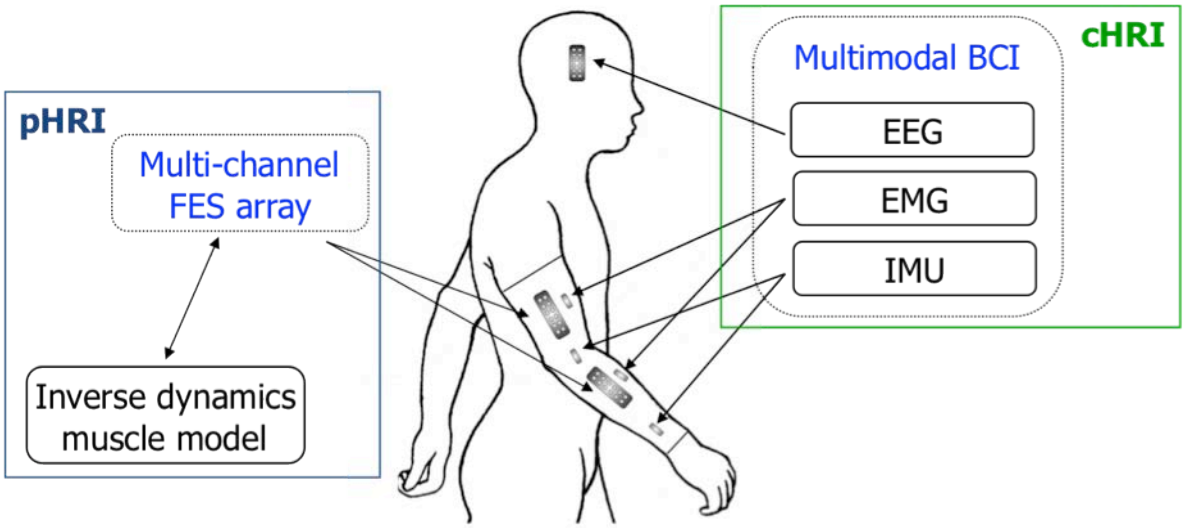

Figure 1. Concept design of the TREMOR neurorobot, showing both physical and cognitive interfaces (pHRI and cHRI respectively).

The BNCI comprises recording of electroencephalographic (EEG) and electromyographic (EMG) activity, together with motion capture with inertial measurement units (IMUs). Each sensor modality aims at extracting certain information, following a hierarchical integration scheme. First, a real–time EEG classifier is in charge of detecting user's intention to perform a voluntary movement, waking up the system. Next, processing of sEMG information yields tremor onset and an estimation of its frequency. Finally, IMUs track instantaneous tremor amplitude and frequency at each joint. This hierarchical integration scheme is summarized in Figure 2.

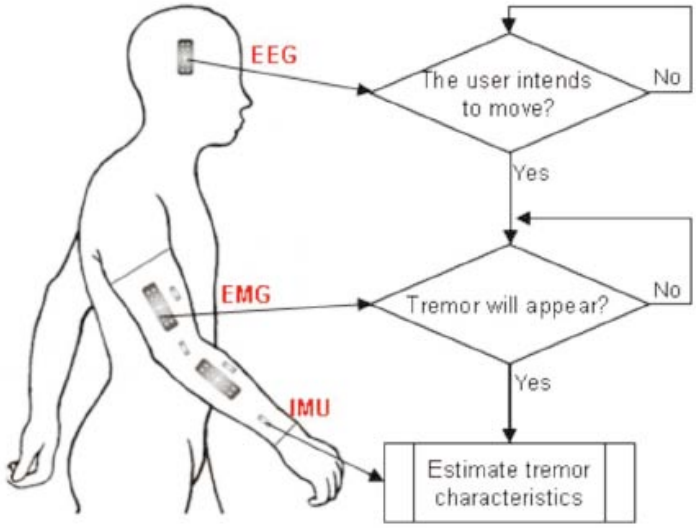

Figure 2. Integration of sensor modalities to drive FES based tremor suppression. First, EEG monitors if the user intends to perform a voluntary motion. Once this has been detected, tremor onset is derived from EMG information . Finally, after the system detects tremor will appear, tremor parameters are tracked based on IMUs.

The use of multiple sensor modalities also permits us implementing fusion and redundancy techniques to enhance the dependability of the system. One example of redundancy is the use of EMG activity to detect the occurrence of a motor command, compensating for eventual EEG classification errors. An example of sensor fusion is the use of machine learning techniques to adjust the parameters of the EEG classifier after the execution of a movement, as detected with IMUs.

This deliverable describes the work developed in WP4: "Multimodal BCI for tremor identification, characterization and tracking". This WP was coordinated by Consejo Superior de Investigaciones Científicas (CSIC) and led by Prof. J.L. Pons. The objectives of this WP are:

(1) To develop a BCI system based on motor bioelectrical activity (CNS and PNS) of the subject. The system should deliver voluntary movement intention and tremor onset at each muscle group in all anatomical joints defined in WP1 and WP2;

(2) To complement the BCI system with biomechanical information (from solid state accelerometers and gyroscopes) to fully characterize tremor at each joint;

(3) To test BCI algorithms both with data obtained from DRIFTS databases (laboratory tests) and with users after programming the BCI on the control architecture of WP3;

(4) To evaluate the dynamics of tremor, i.e. tremor migration and tremor fluctuation, under the application of load.

In order to reach these objectives, the following tasks were defined:

1. *Development of algorithms to identify user's voluntary motor commands.* This task will develop algorithms to be used by the multimodal BCI system in order to identify user intentionality to perform an upper limb voluntary movement.
2. *Development of algorithms to identify tremor onset.* Based on the information provided by the EMG sensors placed over the upper limb of the patient, the algorithms developed in this task will be able to identify the onset of tremor movement.
3. *Development of inertial sensor subsystem.* This task was responsible for the development of the inertial sensor system. This system should provide information about joint acceleration, velocity and position.
4. *Development of algorithms for tracking and extraction of tremor characteristics.* Algorithms for tracking and identification of tremor characteristics based on the information provided by the inertial sensors at each anatomical joint will be developed in this task.
5. *Algorithms for modality fusion.* A sensor fusion scheme from the different modalities (EEG, EMG and IMU) will deliver to the controller the required information to the controller.

The next sections of this document will describe the work carried out in each of these tasks.

2. Development of algorithms to identify user's voluntary motor commands

This section summarizes work on task WP4.1 named *Development of algorithms to identify voluntary motor commands*. This task aims at developing a BCI system, based on the motor bioelectrical activity of the user, which should deliver voluntary movement intention.

This task is led by CSIC, and three partners have taken part in it, ULB, URT, and CSIC. The partners have held a number of telemeetings in order to coordinate and exchange information. Moreover, to maximize the outcome of the work of the different partners, CSIC proposed to adopt a standardization of the experimental and analytical procedures consisting of: defining a common set of experimental and recording options, creating a shared experimental database, testing on it any proposed algorithm, sharing partner experiences, selecting the most effective algorithms, and integrating the resulting ones.

In order to develop the algorithms that identify intentionality to perform voluntary movements in tremor patients, the following work plan was followed:

- Specification of the *requirements* for the identification procedure to be implemented
- Searching a *detectable physiological phenomenon* that informs about the patient motor intention and that fulfills the requirements
- *Designing* a *standard experimental protocol* to collect data from patients
- *Analysis* of the collected data, proposal of a reliable *identification procedure* based on that phenomenon, and *testing it* both on patients and control subjects performing motor tasks habitually used in clinical assessment of tremor.
- *Identification*, based on the previous analyses, which approach provides the best solution for the detection of movement intention in tremor patients.

The physical requirements for the BCI —minimal risks, low cost, portability, high temporal resolution, and fast time response— were early considered during the project proposal preparation, when EEG was selected as the most appropriated technique to implement the BCI. In the current project stage, the following additional requirements were specified for the identification procedures according to our goal and application context:

- Reliability
- Predictability

The identification of the voluntary motor commands must be reliable and, in particular, robust against the involuntary movements (tremor). To meet this goal two actions were taken: using state of the art identification procedures and redundant information sources (EEG + sEMG + IMUs). On the other hand, the voluntary motor command identification also must be predictive in order to allow an anticipative control for the tremor suppression machinery. The fulfilling of this requirement again relied on the current knowledge on EEG.

State of the art

There are a number of physiological phenomena that are related to the preparation, execution, and posterior return to basal brain activity, which are reported in the literature. The most studied phenomena are the readiness potential or Bereischaftspotential, [76], the event related desynchronization and resynchronization (ERD / ERS), [72], and the changes in corticomuscular coherence, [75]. All these phenomena were considered as potential features to develop our algorithm to detect movement intention. It should be notice that, to the partners' knowledge, no work focusing on prediction of movement execution is reported in the literature.

The BP corresponds to the early stage of the Movement Related Cortical Potentials (MRCP), which are the variations of the DC amplitude of the EEG signal related to the execution of motor. The BP consists in a reduction of the DC signal amplitude preceding a voluntary movement. This phenomenon is also divided in two intervals: the "early BP" and the "late BP". The "early BP" begins about 2 seconds before the movement onset, and is more prominent over the presupplementary motor area (preSMA) and the supplementary motor area (SMA). Before the movement onset (400 ms of anticipation), a steeper decay of the DC signal amplitude, which corresponds to the second stage of the BP, the "late BP", can be observed. This second variation of the DC signal slope is best detected over the primary motor area (M1), [69,76].

Oscillations at ~20 Hz in the EEG in humans are coherent with the surface electromyogram during sustained contractions. This is normally designated as CMC, [1, 71]. This observation indirectly indicates the effective

transmission of cortical activity through the corticospinal tract and the monosynaptic connections between cortical neurons and spinal motorneurons, [72]. As the cortico-muscular coherence represents the linear coupling between EEG and sEMG signals in the frequency domain, in the literature, coherence contributions in the beta band (15-30 Hz) have been associated to voluntary movement and thus used as a detection index for the movement intent.

The ERD is also a neurophysiological phenomenon that anticipates the voluntary movement. The ERD refers to the decrease of the EEG signal power in the alpha and lower-beta bands related to the performance of motor tasks, [11]. It begins about 2 seconds before the movement onset in the case of voluntary movements. This desynchronization normally begins over the contralateral hemisphere for movements performed with the dominant arm. The cortical oscillations are supposed to be the means by which the different regions in the brain communicate with each other. The frequencies at which this communication takes place depend strongly on the size of the pool of neurons working synchronously, and on the distance between the brain regions participating in the specific mental task. The specific case of planning a motor task increases the complexity of the neural networks in the motor cortex and smaller parts of this region become more specific. This causes a decrease of the power in the alpha and lower-beta bands within the motor cortex and an increase of power in higher frequencies, in order to reduce energy consumption while performing the task optimally, [74].

The specific characteristics of the ERD have been well studied during the last decades, [11], and many BCI systems are based on this feature of the EEG signal during movements, [8, 75]. Nevertheless, only a few studies with ERD take advantage of its anticipatory characteristic, and most of them present synchronous-BCIs discriminating between pre-defined tasks, [70]. In the present year, a system developed by Bai et al., [73], presents an online asynchronous BCI detecting the movement intentionality with healthy subjects (to our knowledge, no other studies have been published facing this paradigm so far). The system evaluates the best features of the signal spectrum and decides whether a voluntary movement is about to be performed. However, this work has only been tested with control subjects (22.6 +/- 2.4 years old), including a visual system to avoid performing movements when artifacts are measured and using 27 electrodes for the calibration session, which takes up to 30-40 minutes. The system proposed by Bai et al. aims at reducing false positives, which can be an important criterion for systems that only depend on the EEG measurements but not for applications including redundant information of the motor activity from different sensors placed on the body, as in the case of the TREMOR neurorobot.

Moreover, we have identified the following requirements for the specific context of TREMOR project:

- Robustness against tremorous movements.
- Voluntary movement detection must be predictive, in order to allow an anticipative control.

In agreement with this, we decided to base the identification procedure on the event related desynchronization and resynchronization (ERD / ERS) phenomena that underlies the motor activity. Both are observable on the EEG central mu rhythm, whose features were first described by Gastaut et al. in 1952. Since then, the behavior of this rhythm with regard to voluntary movements has been largely studied. Interestingly, mu rhythm changes from a synchronized into a desynchronized mode when a voluntary movement is initiated, and the ERD precedes about 2 seconds the movement onset. The other two phenomenon were discarded due to the following issues:

- *Bereitschaftspotential*. This potential was initially considered since it starts about two seconds before the movement onset. It was not used finally because of its large time-constant.
- *Cortico-muscular coherence*. URT carried out a preliminary evaluation of this approach. They concluded that its high computational requirements hinder its application in real time scenarios. Annex 1 summarizes the evaluation performed by URT of this technique.

Intention detection is facilitated by the stated knowledge about brain topography, signal amplitude, and frequency response of the ERD in the generality of healthy people. Nevertheless, the feasibility to detect the patient's motor intention heavily depends on the extent to which the EEG patterns associated to ERD can be reliably recognized automatically. The main obstacle to achieve this goal is that these patterns are contaminated by spontaneous EEG activity, and the resulting signal to noise ratio is very low. Other immanent problem to the technique is the variability among subjects. Being an additional obstacle, specific for our project, the brain damages and alterations suffered by tremor patients, and the lack of knowledge about how they could affect the ERD/ERS phenomenon.

2.1. Experiments

After selecting the neurophysiological phenomenon, there are still many possible identification strategies that could be considered. This makes it difficult to share experiences among partners and to integrate separately developed algorithms. Therefore, CSIC proposed to adopt a standardization of the experimental and analytical procedures consisting of: defining a common set of experimental and recording options, creating a shared experimental database, testing on it any proposed algorithm, sharing partner experiences, selecting the most effective algorithms, and integrating the resulting ones.

The experimental protocol was designed by CSIC with inputs from ULB and URT. It defined very thoroughly: instructions to patients, tasks to be carried out by patients, number and frequency of the movements to perform, movement amplitude and speed, clues given to patients during the task performing, exact timing for each and every event, etc. The data-recording configuration specified: magnitudes to be acquired, sensor and electrode locations, references and ground locations, sampling rates, on line-filtering, etc. The experiments were designed in such a manner that could facilitate the later investigations on the detection of the movement intention in patients affected by tremor.

2.1.1. Patients

Up to now, two series of experimental sessions have been arranged in the frame of the TREMOR project; both of them were held in Brussels Hopital Erasme with controls and patients suffering from pathological tremor.

6 patients and 3 controls participated in the first series of experimental sessions (January, 2010). Four more patients (3 of them also measured in the first sessions) participated in the second series of sessions (March, 2010). The following tables summarize the clinical information of the patients that participated in the study.

Patient	Sex	Age	Kind of tremor	Grade of tremor (max)	Schwab and England ADL	Nourie-Lincoln ADL
001	M	82	Rest, portural and kinetic	2	70%	18/22
002	M	74	Rest and postural	2	100%	22/22
003	F	61	Postural and kinetic	2	90%	22/22
006	F	34	Postural and Kinetic	1	80%	17/22
007	M	52	Rest and postural	3	80%	19/22
008	M	48	Postural and Kinetic	2	60%	20/22
009	F	74	Posural and Kinetic	1	80&	18/22
010	M	65	Kinetic	2	30%	3/22
012	M	37	Rest, postural and kinetic	4	50%	11/22
014	M	23	Rest, postural and kinetic	2	80%	21/22

Table I. Clinical information of the patients included in the study. The functional scales used to evaluate the patients were described in deliverable D1.1.

Number of patients	10
Age (mean±SD)	55±19.5
F/M	3/7
RSchawab and England ADL score (mean±SD)	72 ± 20.4
Nourie-Loncoln ADL score (mean±SD)	17 ± 5.9

Table II. Summary of the patients included in the study.

2.1.2. Protocol

The protocol followed was first tried with healthy volunteers to assert its feasibility in terms of duration, fatigue generated and ease of execution. A flowchart describing a series of sessions is represented in Figure 3.

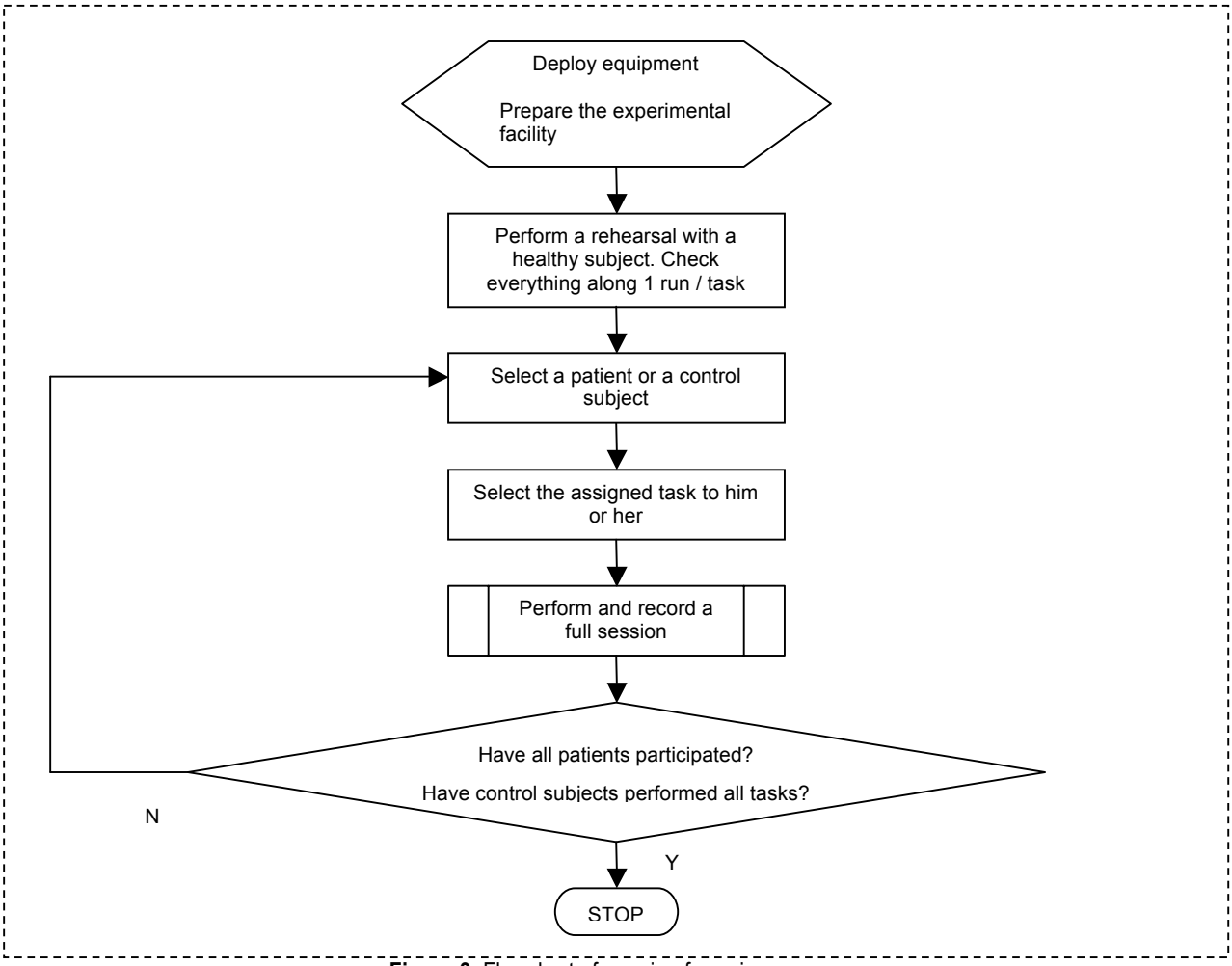

Figure 3. Flowchart of a serie of sessions.

During the experiments, each patient measured was sitting in a comfortable chair while the technicians placed the equipment in a correct manner. Before the recording started, the patient was asked to avoid artifacts (like eyes blinking, eyes moving or chewing) and to remain still, without moving any part of the body but the limb with which the task had to be performed. The preparation time took an average of 1 hour and a half per patient. After it, 6 runs of repeated task executions were accomplished. A resting time was stablished every two runs to avoid patient's fatigue (Figure 4).

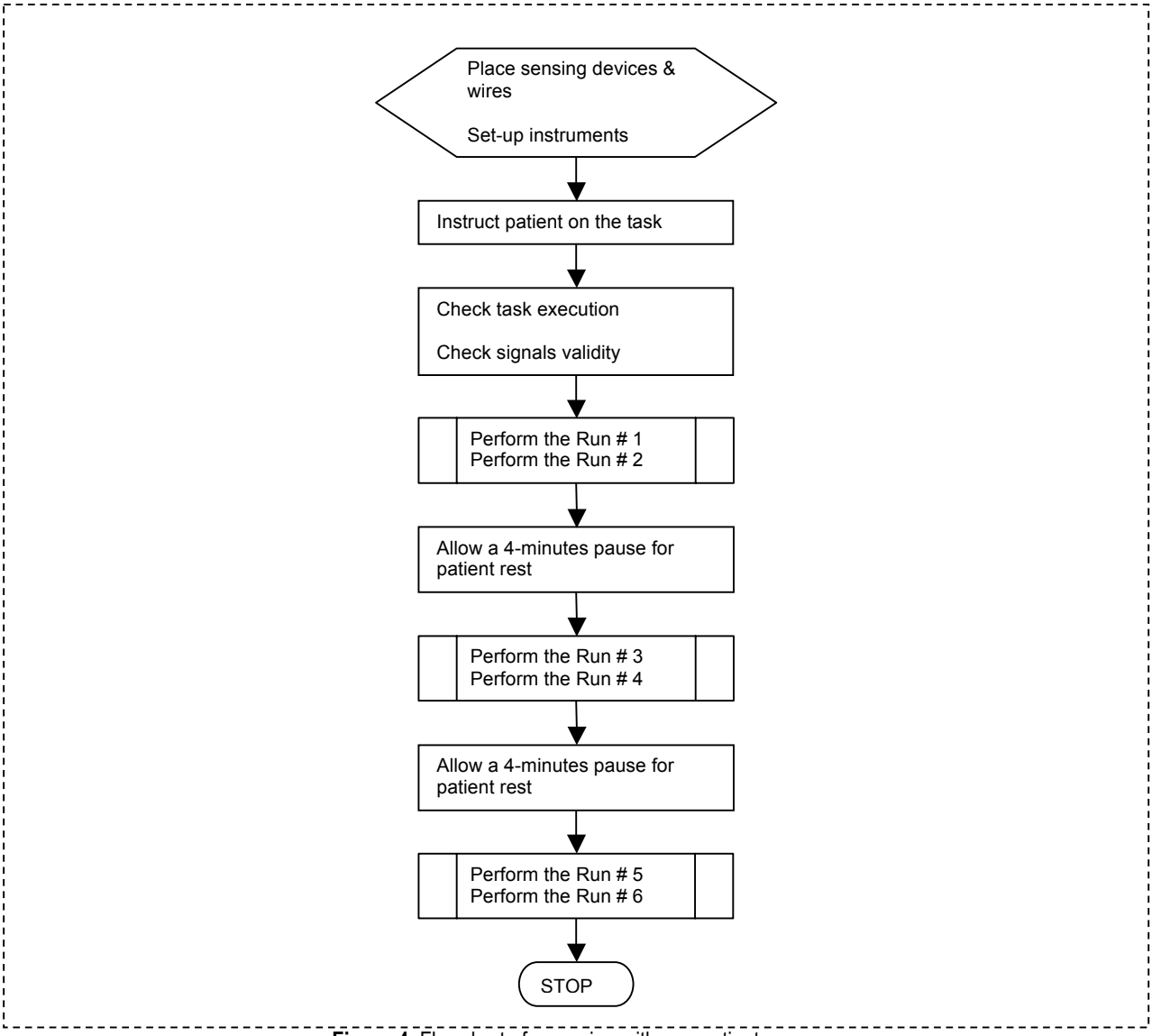

Figure 4. Flowchart of a session with one patient.

In each one of the 6 runs, the patients were asked to stay steady and to perform periodically a motor task consisting of driving the right hand index to the nose and back to the rest position (Table I). An acoustic reference was reproduced 10 seconds after each movement onset to indicate the subjects when they could start with a new trial. This reference assured a long enough separation between two consecutive trials for the patient's brain to get back into a basal state.

Subjects were requested to wait for a short period of time after each acoustic reference. The movement executions that didn't satisfy a condition of more than 3 seconds between the acoustic indication and the next movement were removed in the posterior analysis (typically, the desynchronization in voluntary movements starts 2 seconds before the onset of the movement, [8], and the duration of the evoked potential caused by the acoustic reference is less than 1 second).

Thus, each valid trial consisted of an initial acoustic reference time followed by a self-chosen period of no motor activity (higher than 3 seconds), an execution of the motor task and an additional period of time of no motor activity (Figure 5).

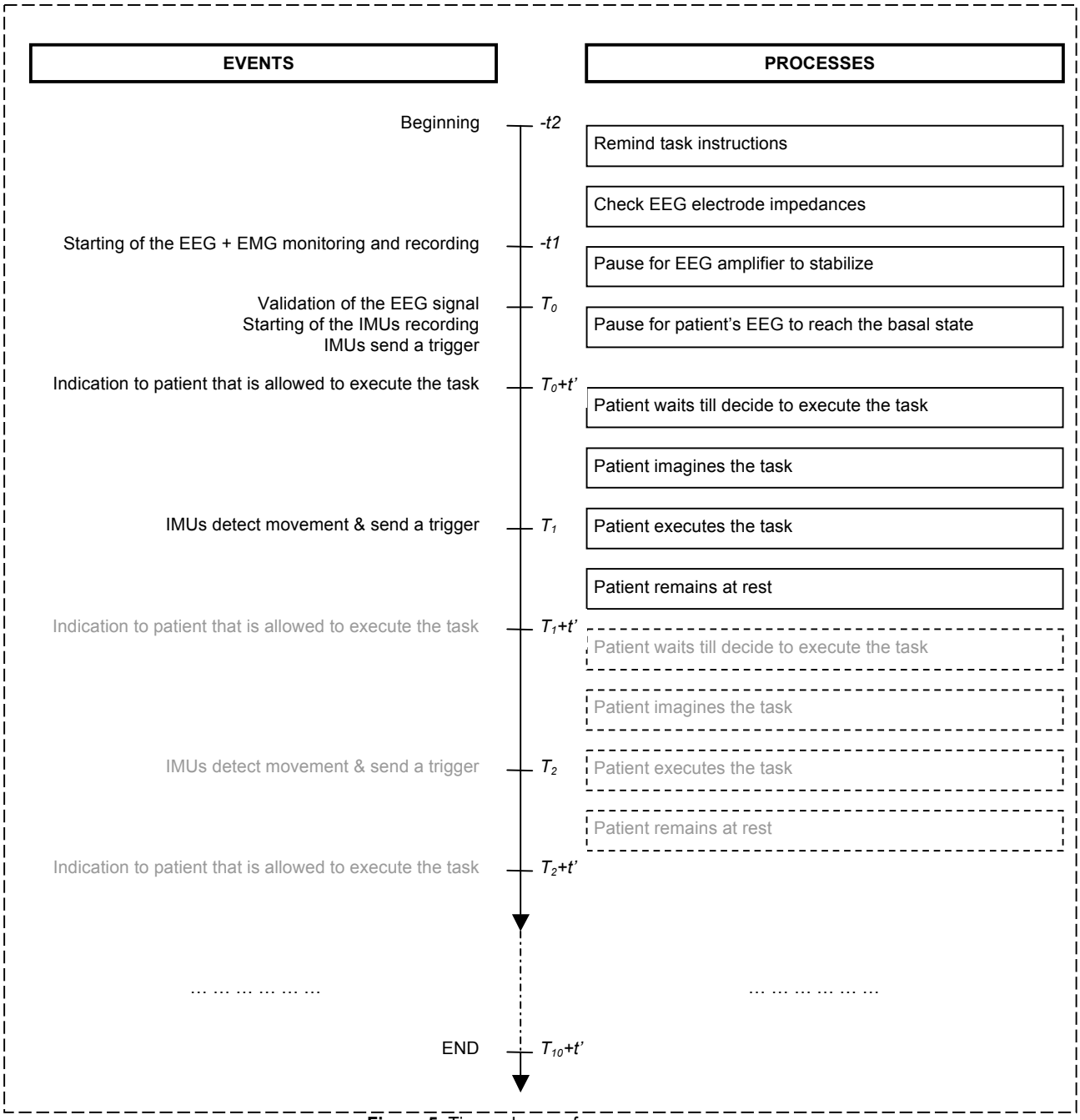

Figure 5. Time scheme of one run.

A total of six sessions of 3 minutes and 30 seconds were recorded for each patient, which resulted in an average set of 60 trials performed by each one of the measured patients. The average time between movement executions was 22+/-7 s.

Seat type	Chair
Resting position	Comfortably seated and relaxed
Arms and hands	The ulnar part of the hand is touching the distal third region of the thigh (tape on thigh for localization)
Legs and feet	Feet rest over marked positions on the ground
Task	
Description	At a self-chosen moment, after about 5 seconds of hearing the acoustic indication, the patient imagines and immediately afterwards with the dominant arm executes the task by touching the nose with the index finger. The movement starts from, and returns to, the rest position on the thigh.
Specifications	The index is pointing forward initially. The index has to touch the nose, to remain on it for about 1 second and then to come back to the thigh at the starting position. Examiner asks the subject to perform the movement slowly and with accuracy
Patient instructions	Acoustic indication: "*allez-y*"
Body control during tasks	Eyes open. Mouth lightly opened. Jaw relaxed. Restrain any head movement. Avoid blinking and swallowing. It is mandatory to imagine and execute the task at least 3 seconds after the acoustic indication.

Table III. Specifications for task finger-to-nose (FN)

2.1.3. Sensors

EEG signals were recorded from thirteen positions over the motor area (FC3, FCz, FC4, C5, C3, C1, Cz, C2, C4, C6, CP3, CPz and CP4 of the international 10-20 system) (Figure 6) with a gTec amplifier and Au scalp electrodes. The reference was set to the common potential of the two earlobes and POz was used as ground. The amplifier was set to filter the signal between 0.5 and 60 Hz, and an additional 50-Hz notch filter was used.

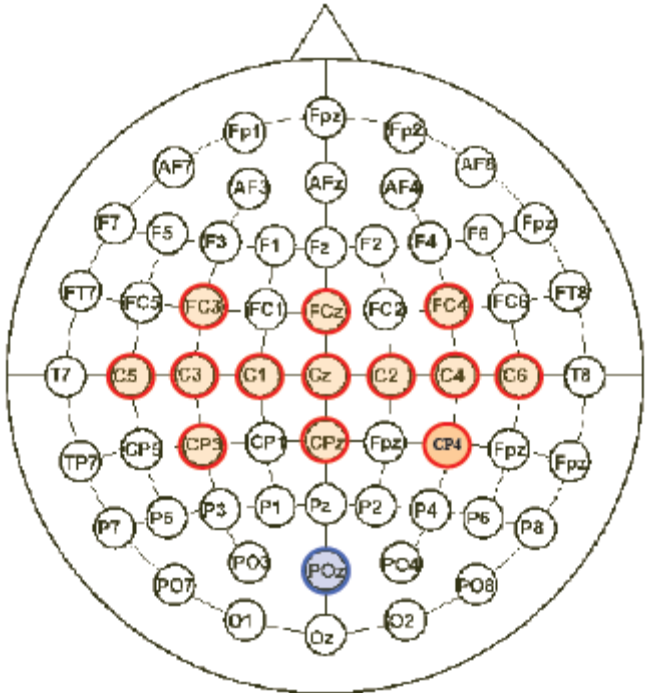

Figure 6. Electrodes placement

Synchronized with the EEG acquisition, movements of the right arm and hand were characterized by means of EMG (EMG-USB amplifier OT Bioelettronica, Torino, Italy) and inertial sensors (manufactured by Tech MCS, Madrid, Spain). The inertial sensors communicated with a PC running QNX Neutrino (QNX Software Systems, Ontario, Canada), which was also in charge of sending the synchronization pulse at the beginning of each run to the two amplifiers (EEG and EMG) and a set of pulses each one of them corresponding to each movement onset detected (Figure 7). For more information on the measurement platform please refer to deliverable D7.1.

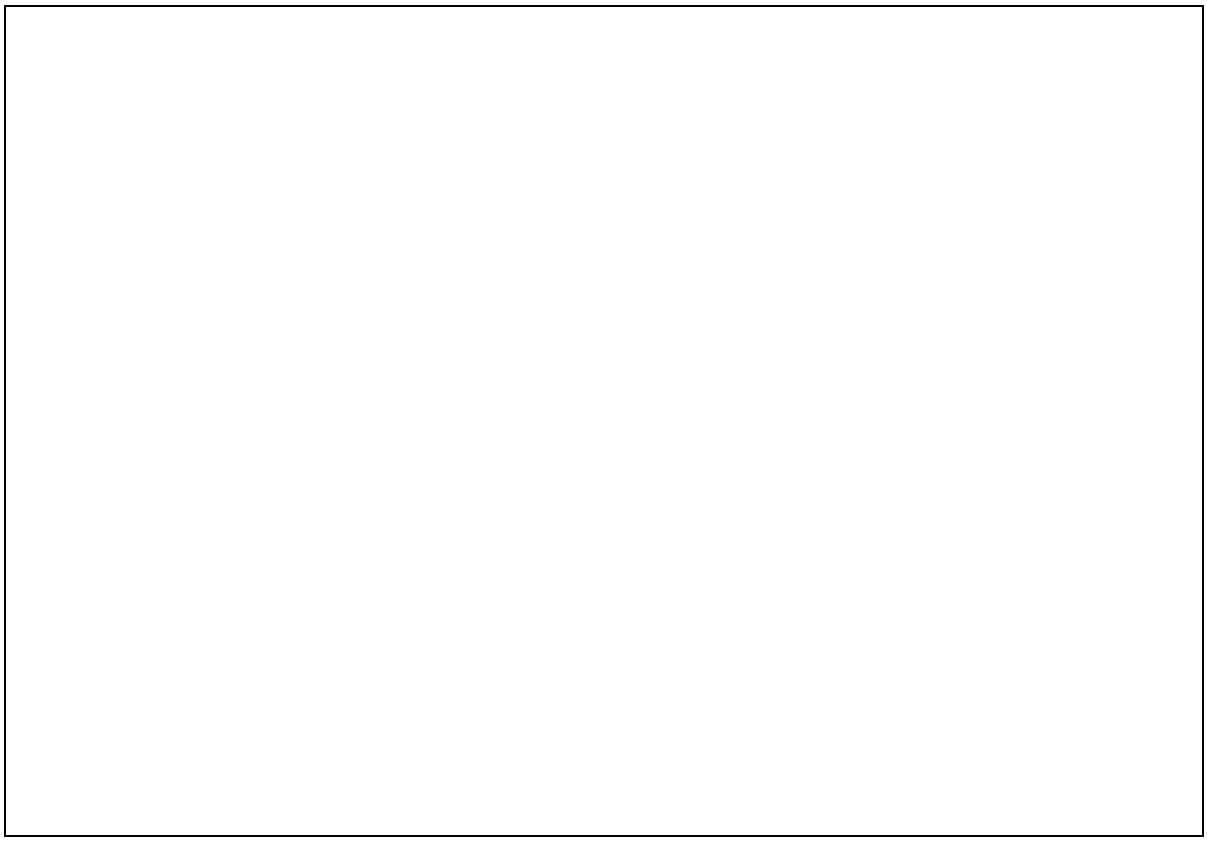

Figure 7. Scheme of the interconnected measuring devices.

The data including the EEG recordings, the times at which the movement onsets were detected and the acoustic references was stored at a sampling frequency of 256 Hz for posterior offline analysis (Table IV). Likewise, the EMG data of the four muscular groups involved in the FN task (extensors, flexors, biceps and triceps) was stored at a sampling frequency of 2048 Hz including the initial synchronization pulse (Table V). Finally, the inertial sensors information of three points in the right arm was stored at 50 Hz (Table VI).

EEG electrodes type	Conventional, passive Au electrodes
EEG electrode locations	FC3,FCz,FC4,C5,C3,C1,CZ,C2,C4,C6,CP3,CPZ,CP4
Ground location	POz
Reference location	Linked ear-lobes
EOG electrode locations	At the right eye: 1 below + 1 on the right
Sampling rate	256 Samples / second
EEG Filters (type/band)	Notch for 50Hz. Band-pass for 0.5–60Hz
EOG Filters (type/band)	Notch for 50Hz. Band-pass for 0.5–60Hz

Table IV. EEG sensors placement and amplifier configuration

EMG electrodes type	Semi-disposable adhesive EMG matrices
Location(s)	- biceps brachii - triceps brachii - flexor carpi radialis - extensor carpi ulnaris
Sampling rate	2048 Samples / second
Reference location	Wet wrist bracelet
EMG Filters (type/band)	Band pass for 10 - 750 Hz.

Table V. EMG sensors placement and amplifier configuration

IMU sensors type	Each IMU contains 3D accelerometer, gyroscope, and magnetometer
Location(s)	- Third metacarpal. - Edge of the forearm, dorsal side. - Olecranon process.
Sampling rate	50 Samples/ second
IMU filters (type/band)	None

Table VI. Inertial sensors placement and configuration

2.2. Data Analysis

The main role of the EEG-based detector developed in the TEMOR project is to provide information about the movement intention of the subjects measured. The system must be able to work continuously and be a usable solution for activities of daily living. This requirements lead to two main consequences that have been addressed in our proposal:

- The *reduced* number of electrodes used allows the system to be thought of as a daily usable solution, as stated in the DoW.
- The *system* is specifically developed for running online, continuously checking whether the cortical electrical activity measured corresponds to a premovement state and avoiding the usage of external cues as timing references, which means that our EEG based detector works as an asynchronous-BCI, [9].

As the detector is supposed at first to work at the same time as the inertial and EMG sensors, its contribution to the global system relies on the principal lack of these other two sensing devices: motor activity characterization by means of IMUs and EMG can only be achieved once the movement has been initiated, so the anticipative feature of the ERD phenomenon is the main criterion for developing and optimizing the EEG-based detector.

Moreover, as the detector system must be capable of working on different subjects, it has to be able to adapt its internal processing and classifying parameters to each specific person wearing the system, and this is also an essential aspect addressed in our detector design.

2.2.1. A Bayesian Classifier to Detect Event Related Desynchronization

In order to fulfill the previous requirements, CSIC has developed a Bayesian classifier assessing features as the absolute power of the EEG signal over the motor area in subject-dependent locations, time-windows and frequencies. The main advantages of a Bayesian classifier are that it is computationally efficient and it easily allows being online configured, adapting its parameters to the ongoing measurements.

Finally, as will be pointed out in the results section, since the classifier is going to work online and continuously, its validation will be based on events instead of performing a classical sample-by-sample analysis.

System description

From the literature referring to the ERD phenomenon and our own experience analyzing the EEG data of patients with pathological tremor during consecutive executions of movements, the main issues to take into account when characterizing the ERD in the intervals of EEG data preceding a certain voluntary movement are:

- This desynchronization is best seen over the motor area, and it presents different desynchronization patterns in the ipsilateral and the contralateral areas;
- It may be detected in both the alpha and beta bands and the specific frequencies at which it is most prominent are subject-dependent;
- The desynchronization lasts around 3-4 seconds when executing simple tasks and this length changes for each trial and between subjects.

These three characteristics show a certain degree of variability among subjects, so it becomes important to adapt the classifier for each subject measured, using as training reference the previous trials measured in a scenario where the classifier works continuously.

The Bayesian classifier we propose is based on these relevant aspects and it learns online its internal parameters in order to detect the desynchronization phenomenon the best way possible. Thus, the classifier looks for (Figure 10):

- The frequencies in the alpha and beta bands at which the ERD phenomenon is best observed (Figure 8);
- The electrode positions where the highest differences (in the optimal frequencies), between the basal (resting period) and movement states are found (Figure 7). As a Laplacian filter is used to improve the spatial resolution, in this step the electrodes analyzed are C3, Cz and C4 (these are the only electrodes that can be spatially filtered since they are the only ones surrounded by four other electrodes, as can be seen in the experimental setup described in the previous section (Figure 6));
- The best time window length for estimating the desynchronization (Figure 9).

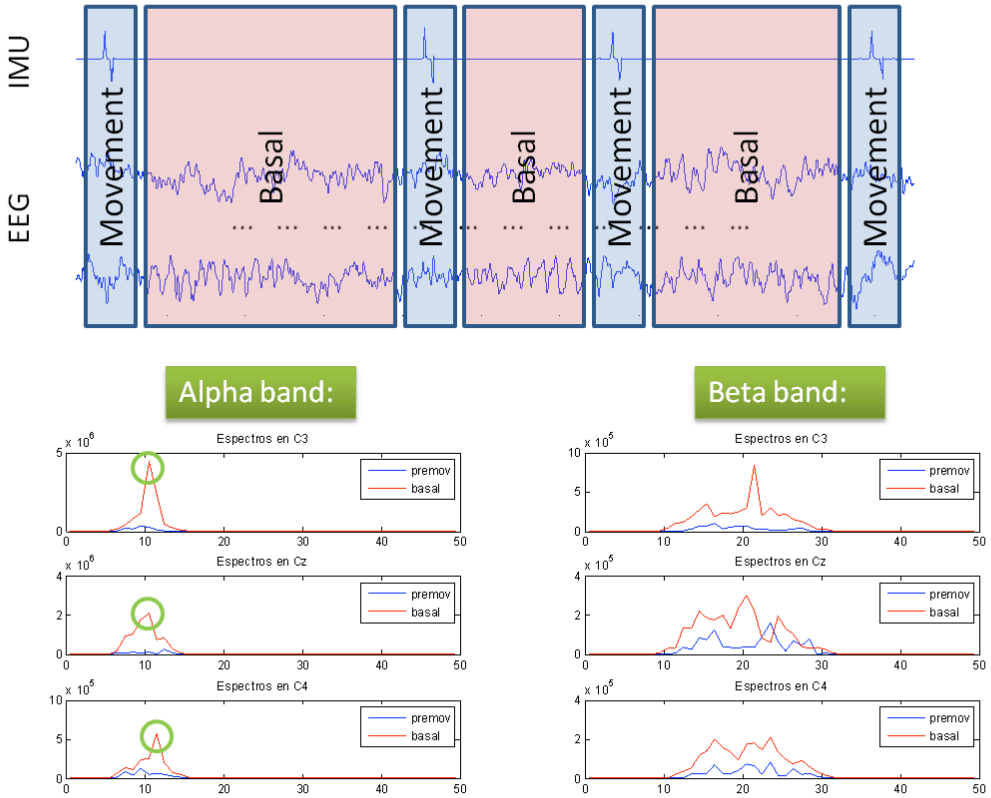

Figure 8. Scheme of the automatic detection system of the optimal frequencies and channels. The EEG data of a specific subject measured is first divided into basal and movement intervals (top). The comparison of spectra of the basal and the movement states is carried out along the different channels and frequencies to detect which combinations of these two parameters are optimal in terms of the two states distinction (bottom).

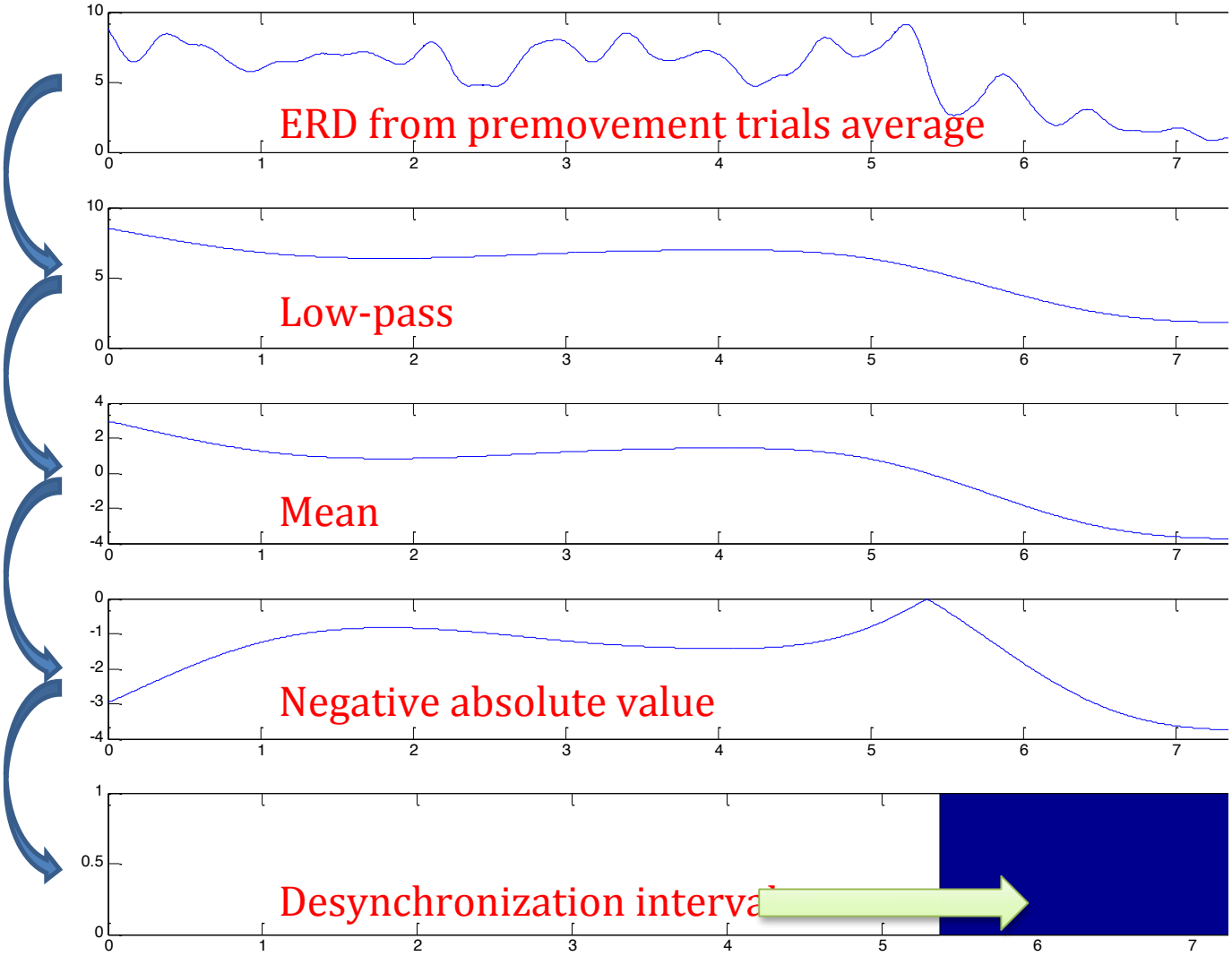

Figure 9. Automatic detection of the observing window length.

The selection of optimal frequencies, channels and time windows is accomplished online, by processing the movement intervals of the previous trials acquired, Figure 10. The time locations of these previous movement executions are obtained from a control signal received from the IMUs block, which reports the onset of each one of the movements executed, Figure 7.

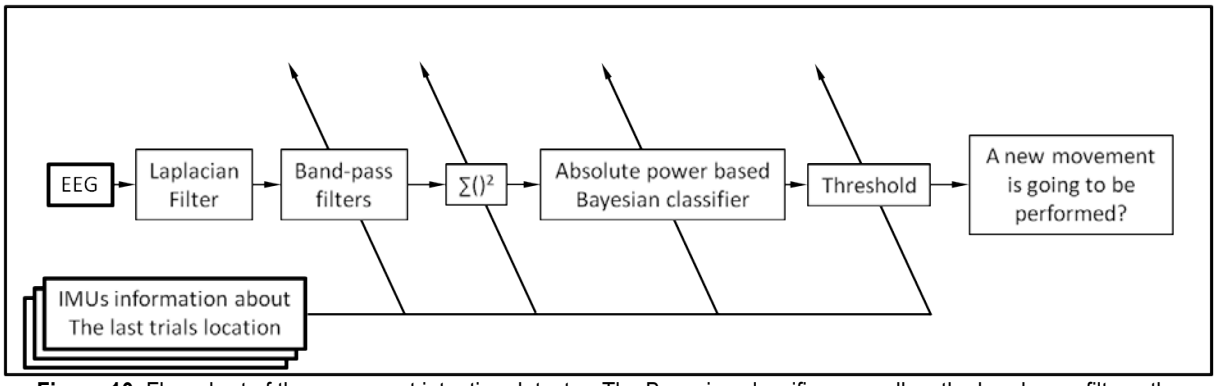

Figure 10. Flow chart of the movement intention detector. The Bayesian classifier, as well as the band-pass filters, the threshold and the time window for power estimating are updated by means of the IMUs feedback.

The Bayesian classifier is used for determining whether a movement is about to start. It uses as input features the absolute power in each combination of the optimal channels, frequencies and time windows. The output probability of the classifier is then converted into a binary signal by applying a threshold, which is selected by

defining the minimum recall accepted when classifying the training dataset (where recall is the amount of movements anticipated and will be further specified in the results section).

In order to train the classifier, the absolute power measured of the previous movements is used to generate the probability curves for the absolute power in each channel-frequency combination.

This implementation of a Bayesian classifier evaluating the absolute power of the alpha and beta rhythms gives rise to an automatic system with low computational load when classifying in real-time.

Results

The results shown here have been obtained by means of an offline 5-fold cross-validation test among the six 3-minute sessions of each patient (as described in the protocol section).

Each classification of a session uses as training dataset the pre-movement time windows of the movements performed in the rest of the sessions. The test sessions are classified continuously (the complete 3 minutes and 30 seconds session is analyzed, as in an online scenario), without removing artifacts. The intervals where the acoustic references sounded aren't removed either.

In order to evaluate the classifier performance we select an analysis mode based on events instead of a sample-by-sample test. This means that the parameters selected for the validation and optimization of the detector are based on activation units (AU), which are the temporal intervals in which the classifier identifies the premovement state with a probability over the decision threshold. The reason why we evaluate the events of classification instead of the samples is that a group of consecutive single activations of the classifier are likely to correspond to a same process in the cortical activity (which tends to vary at a slow rate in comparison with the classifier), so these consecutive activations must be considered as a singular classification, [10].

According to this approach, we define the conditions for an AU to be classified as a true-positive classified event (TP) or as a false positive classified event (FP) and two indicators for testing the classification results based in these two values:

$$Precision = {}^{TP}/_{(TP+FP)};$$

$$Recall = {}^{TP}/_{(TP+FN)};$$

Where

TP (true positives): number of AUs intersecting or containing the interval [−0.5 : 0].

FP (false positives): number of AUs intersecting the interval (Movement Ending : −0.5).

FN (false negatives): number of non detected movements.

Activations which are only present during the movement execution aren't taken into account

The criteria chosen for defining an AU as a TP or FP fit the classifier specifications and the training characteristics of our detector: the aim is to detect a movement before it is performed and thus the movement preceding intervals are chosen for the training stage.

Based on these criteria, the results achieved for the four patients are shown in Table 5 where the Precision and the Recall results are obtained over the 6 test sessions measured with each one of them. The classifier is able to anticipate 85% of the movements executed in the best case (patient 4), generating a small amount of wrong activations. An average precision result of 46.5% represents a reduced percentage of false activations considering the fact that, during the protocol proposed for this study, the 82% of the time represents a basal state of the subject, while the pre-movement condition is found just in the 2% of the time measured (the rest 16% of the time corresponds to the movement intervals). A classified run of the patient 4 is shown in Figure 11.

Patient	Precision	Recall	Mean AU length	Mean anticipation
1	45%	50%	1.41 s	0.29 s
2	34%	75%	0.45 s	0.55 s
3	47%	68%	1.70 s	0.16 s
4	60%	85%	1.76 s	0.30 s
Average	46.5%	69.5%	1.33 s	0.32 s

Table V. Results for four patients

Moreover, it can also be seen in Table V that the anticipation of the movement detection is for most of the cases higher than 250ms and the length of the activation units takes values around 1.3s. These results reflect the high accuracy of the detector for time location and anticipation of movement onsets.

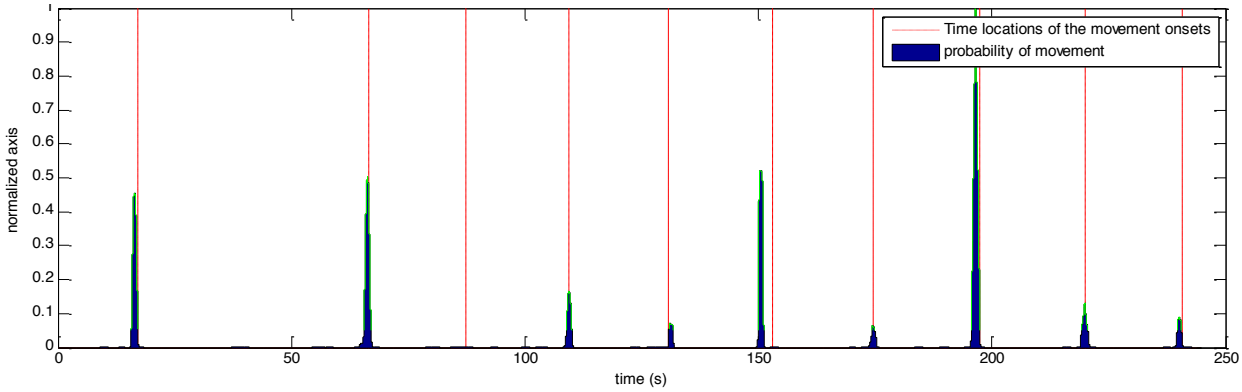

Figure 11. Example of a classified session for patient number 4. Gray discontinuous vertical lines indicate the locations of the voluntary movement onsets (based on the IMUs information)

Finally, it would also be important to track the motor cortex electrical activity during tasks executions different from the one proposed in this document consisting of performing a voluntary movement after long periods of inactivity. Some different situations that would be interesting to characterize are:

- The intervals of time at which the subject wearing the system is being stimulated;
- Motor tasks switch without stopping into a resting state between the two tasks;
- Tasks execution in time intervals shorter than the 20 seconds periods found in our protocol proposal.

2.3. Real-Time Binary classifier

The work of URT for WP 4.1 has been focused on the development of a real-time binary classifier based on an algorithm for the detection of ERD events as onset for the voluntary activity performed by the patients. The binary classification is able to distinguish, on a sample-by-sample basis, events related to movement intention from no-movement status. The design of the algorithm is based on the well-known method proposed in [11]. Traditional methods for ERD/ERS detection are based on off-line averaging tecniques applied to the EEG power in alpha band, by using a series of triggered successive trials. This kind of approach is not suitable for the implementation in the TREMOR framework, where a real-time approach is needed.

The implemented algorithm is based on the real-time envelope estimation of the power of the dereferenced EEG signal in the alpha band. ERD events are then detected when significant decreasing patterns of the signal power, with respect to a threshold calculated on a dynamically updated baseline, are present. With this approach, patient training is not needed.

Details on the flow-diagram of the algorithm are described in the following:

- EEG signal is dereferenced by means of a mean average reference algorithm, that is by subtracting the weighted contribution of all the recorded electrodes to the electrode chosen for the analysis. This procedure allows reducing the influence of fluctuations on the reference electrode in monopolar EEG montages. Implementation choices included using C3 and C4 as the electrodes undergoing the subsequent analysis.

- Dereferenced EEG signal is then band-pass filtered in the upper alpha band (10-12 Hz) and squared, in order to obtain its power.
- The latter is then low-pass filtered by means of a two-stage filtering unit, including a non-linear and a linear filter. In the first stage, within an observation window of 8 samples, its central sample value is replaced with the range value. The second is a 0.1 Hz 1st order Butterworth low-pass filter and is cascaded to the previous filter. An alternative implementation of the algorithm uses a critically dampened filter, [12], instead of the two-stage unit, giving similar results in terms of estimation delay and envelope estimation accuracy.
- The processed signal is then used for ERD detection: a baseline value, associated to a no-movement status, is calculated on a dynamic window of variable length, lasting maximum 4 s; if the value of the processed signal is below 70% of the baseline for more than 250 ms, then an ERD event is detected and associated with movement intention onset class.
- Two different methods have been implemented for voluntary activity offset detection. In the first one, the offset of the voluntary activity is detected from the processed EEG signal, when its value exceeds 70% of the baseline for more than 250 ms, [13]. In the second approach, [14], the offset of the voluntary movement is identified by revealing sEMG activity offset for the relevant muscle, using a standard algorithm for muscular activation pattern detection (Hodge's algoritm [15]).
- When the offset is detected, the baseline of the processed EEG is updated.

Figure 12. Flow diagram of alpha power envelope estimation for ERD detection

Results

The real-time classification scheme has been tested using data acquired during the consortium aquisition sessions in Bruxelles. Both versions of the algorithm (EEG-based offset detection and hybrid offset detection) have been applied on single wrist movements and on series of finger to nose (FTN) movements (8 to 11 movements with a time span of 20 seconds between two consecutive movements), triggered by an acoustic signal.

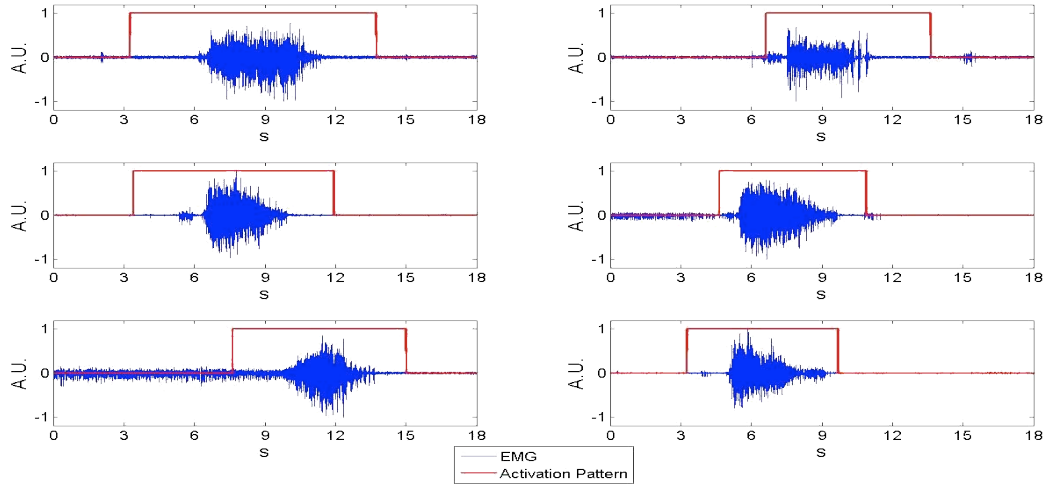

Figure 13. Results for single wrist movement task.

For the single wrist movement task, the correct classification rate reaches 80%, with a mean advance value of 1.59 s and a standard deviation of 1.09 s. Nevertheless, some false positive transitions occurred after the detection of the voluntary movement, possibly associated with the data variability.

For the FTN task, results, in terms of correct classification rate, indicate that about 60% of the movements are correctly detected (the second version of the algorithm showing better performance with respect to the first) with a mean advance value of 5 s with a standard deviation of 2.3 s. These values probably include spurious ERD events associated with responses evoked by the acoustic trigger signal. The percentage of correct classifications underlines and confirms the high variability of the ERD phenomenon also in strictly controlled experimental conditions.

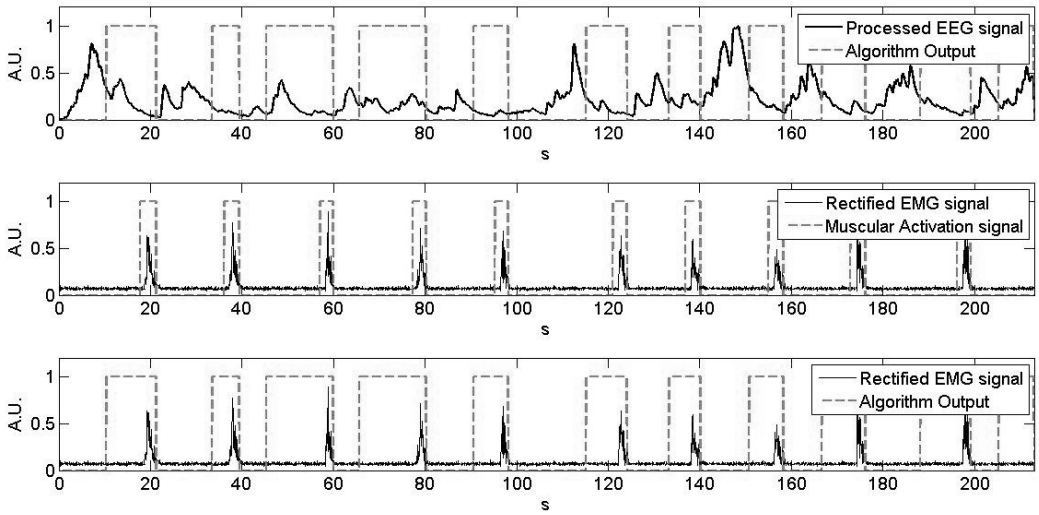

Figure 14. Example of results for FTN task.

2.4. Discussion & conclusions:

The BCI detector of the movement intention proposed in the framework of the TREMOR project must fulfill three relevant aspects:

- It is essential that the detector works online, so that it is able to trigger the tremor cancellation system that tremor patients will wear while performing their activities of daily living;
- The detector must also anticipate the incoming voluntary movements. A minimum anticipation time of 20 ms before the movement onsets is recommended so that the tremor cancellation system (EMG, IMUs and FES) has enough time to model the tremor before actuating;

- Finally, given the information redundancy as a result of measuring the motor activity by means of three different sources (EEG over the motor cortex and IMUs and EMG directly placed on the moving limb), the FP rate becomes a secondary parameter to take care of, since the wrong information coming from the EEG-based detector can be detected and ignored by means of the two real motor measurements coming directly from the limb analyzed. The TP rate, on the other hand, is a crucial parameter to consider and optimize.

These requirements are correctly met by the detector presented in previous sections as could be verified in the results sections. The Bayesian classifier was selected as final solution of TREMOR project due to its self-learning characteristic, which allow the system to adapt to the different users.

Results of this classifier indicated that the amount of time anticipated is, for most of the trials detected, over the minimum time needed in order for this information to be used by the posterior tremor cancellation strategies, and the recall rate achieved shows that for most of the people measured more than 68% of the movements are anticipated.

On the other hand, it is also important to note that the mean length of the AU for the pre-movement detection cases is lower than 1.5 seconds, which means that the time precision of the movement onsets estimations is very high.

It is nevertheless important to point out the variability of the results achieved depending on the patients (and subjects in general). Although most of the people present evident characteristics of desynchronization when averaging among trials, the single-trial classifying results change dramatically from some subjects to others and for patients with no visible desynchronization or with big trial-to-trial variations of the premovement activity, the contribution of this kind of BCI applications may not be worthy.

In order to improve the detector's performance, especially in the aforementioned cases where the desynchronization features aren't as pronounced and stable as desired, two research lines are still to be evaluated. The first one would be to look for new ERD-related features that combined with the one proposed for our detector (the absolute power in specific bands) increased the robustness of the movement prediction. Secondly, a data-mining period with data measured from a particular patient could help detecting from a group of features extracted from the EEG recordings, those that were most relevant in a single-trial classification scenario. This could lead to a much more subject-specific application that could suit optimally each patient's EEG features preceding the execution of voluntary movements.

3. Development of algorithms to identify tremor onset

This section summarizes work on task WP4.2 named *Development of algorithms to identify tremor onset*. This task aims at detecting the onset of tremor from muscular activity recorded with surface EMG (sEMG).

This task was led by AAU, and CSIC and UNA have given support to their work.

The following work plan was carried out:

- To develop a computational model of EMG during tremor, which constitutes the basis upon which tremor characterization algorithms are proposed and evaluated.
- To validate this computational model of EMG during tremor by comparing its outcome with recordings from tremor patients.
- To propose and algorithm for tremor detection out of EMG information, and evaluate its performance with model data.
- To validate the tremor detection algorithm with patients' data.

3.1. Computational model of EMG during tremor

Computational models are valuable tools to analyze interdependences of involved elements in physiological systems, including the genesis of pathological tremor. For example, a model of tremor based on a Hill-type muscle model has been developed to examine the contribution of afferent feedback to centrally generated tremor [16]. Similarly, other modeling studies have addressed the influence of proprioceptive reflexes and the gains in these reflex pathways on motor stability [17-21]. However, previous models do not include the simulations of the single motor unit activity and of the surface EMG signals.

The aim of our novel tremor model was to provide a flexible tool for the generation of surface EMG signals during various types of tremor and in various conditions. The different types of tremor include different frequencies and intensities, while the various conditions refer to varying degrees of voluntary activity. By means of model simulations, a wide range of simulated tremor-EMG signals can be generated easily. On the other hand, collecting experimentally a similar body of data would require a large patient population and a significant amount of time.

The described model was implemented by integrating and expanding a large number of previously proposed models. This work has been presented preliminary at the ISEK and IEEE EMBC conferences conference, [22,23].

Figure 15 depicts the structure of the model for a single muscle. In the present study, the model included two muscles, reflecting the characteristics of the antagonistic muscle pair of the first dorsal interosseous muscle (index finger abductor) and the first palmar interosseous muscle (index finger adductor). Importantly, the model is flexible and expandable, i.e., the other muscle systems, potentially with more muscles, can be simulated by combining several single muscle models and by changing the model parameters. The FDI has been selected for the current (initial) model since it was the subject of a large number of previous modeling studies (e.g. [24-26]), and therefore a highly valid foundation for building the model was already available by drawing from these previous experiences.

The model was structured as a closed-loop system. The net synaptic input for the pool of motor neurons innervating the muscle comprised the following: 1) descending voluntary drive from the motor cortex, 2) afferent feedback activity, and 3) oscillatory tremorogenic input. *Descending voluntary drive* from the motor cortex to the motor neurons of both muscles was continuously adjusted so that the simulated limb angle followed the predefined trajectory representing the volitional movement. This adjustment was performed using a PID (proportional, integral, derivative) control algorithm that was acting to minimize the tracking error, i.e., the angular error between the predefined trajectory and the instantaneous simulated angle. Positive output of the PID algorithm was used as the input for the agonist muscle, while the negative output was used as the input for the antagonist. This type of control algorithm has been already successfully applied to estimate neural input in a previous modeling study by Dideriksen *et al.*, [26]. Apart from the descending drive, afferent feedback was also included as a neural input, since it has been shown that it also contributes to tremor generation, [16]. Muscle spindles, which are sensitive to change and the rate of change of muscle length, were implemented according to the description by Houk *et al.*, [27], while Golgi tendon organs that act like force transducers were implemented as described by Prochazka *et al.*, [28]. Finally, in order to simulate tremor, band-passed filtered white noise was superimposed to the summation of the other types of synaptic inputs. A second-order filter with the width of 1 Hz around the predefined tremor-frequency and with a settable gain determining the desired tremor intensity was used.

Based on the *net synaptic input* the model of the *motor neuron pool dynamics* proposed by Fuglevand *et al.*, [26], estimated single motor unit (MU) spike trains for the muscle (*single MU discharge pattern*). Based on these patterns the surface EMG and the active muscle force were determined. The surface EMG was simulated by using a *model of surface EMG generation* proposed by Farina *et al.*, [29], which allowed simulations of both single and multichannel EMG recordings. In the current configuration, a matrix of up to 11 x 17 electrodes with an inter-electrode distance of 2.5 mm could be simulated. The physiological and anatomical parameters were taken from the study by Keenan *et al.*, [30] that used the same model of the surface EMG to simulate the EMG of the FDI. The active muscle force was estimated by using the model of Fuglevand *et al.*, [26], which was expanded to take into account force-length and force-velocity muscle properties according to the description given by Zajac, [31]. The passive forces due to tissue resistance at extreme limb angles and viscoelasticity (depending on the limb angle and angular velocity) were implemented based on the general description by Esteki *et al.*, [32]. Furthermore, the external forces representing the inertial loading of the limb could be added. The sum of passive, active and external forces determined the net muscle force, which was proportional to the rate of change of the musculotendon length. The *limb angle* was estimated using the laws of trigonometry based on the assigned anatomical properties of the limb.

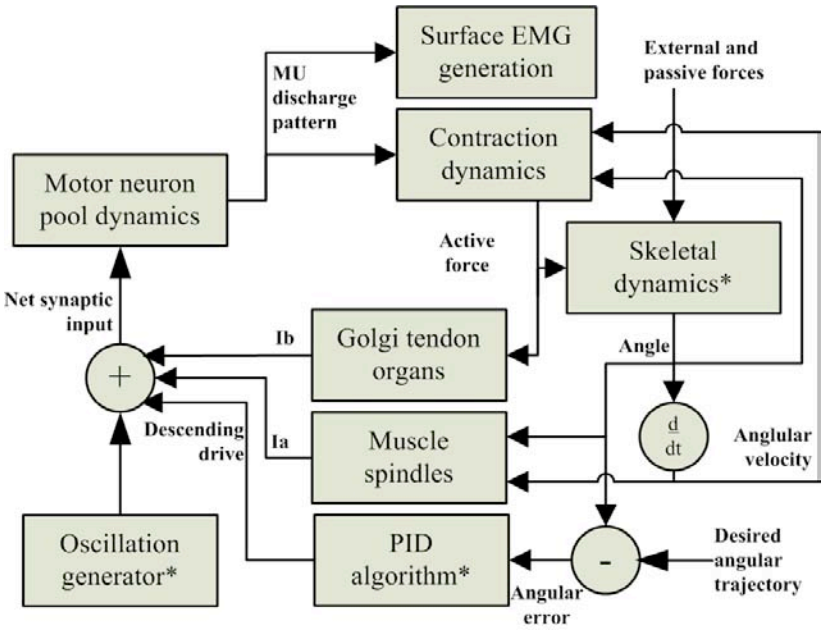

Figure 15. Model structure. Asterisks indicate sub-models that run concurrently in both the agonist and antagonistic muscle, while the other sub-models run separately for each muscle. The model components are described in the text.

3.1.1. Validation

The model was validated by comparing the simulation results to those observed in previously published experimental studies focusing on EMG and single MU activity during pathological tremor.

The characteristics of the power spectral density (i.e., the amplitude and width of the spectral peak) of the surface EMG and the limb angular velocity during different degrees of voluntary activation and at different tremor-frequencies resembled those observed experimentally at low and high contraction levels in three different studies with a total of 82 tremor-patients (mainly Essential Tremor and Parkinson's Disease), [33-35]. Furthermore, the spectral characteristics were similar to those obtained in the study by Zhang *et al.*, [16], in which the simulations were conducted by varying the gains of the afferent synaptic input. Finally, the characteristics of the MU spike trains, visualized by interspike-interval histograms, were similar to those obtained by Christakos *et al.* during isometric contractions across a wide range of contraction levels (2-45% MVC) and with varying tremor-frequencies (19 subjects, tremor frequency 9.2±3.1 Hz), [36].

Figure 16 depicts the simulated angle, force, EMG, and spike train for one motor unit during simulated, sustained 6-degree abduction (voluntary movement) with a moderate degree of 8 Hz tremor. The 8 Hz fluctuations are clearly visible in the simulated angle, whereas the low-frequency oscillations (<2 Hz) are due to the variability in the voluntary descending drive (i.e., the output of the PID algorithm). To maintain this angle against the opposing passive forces, a low degree of voluntary drive was required, which was reflected in the fact that the mean force was ~8 % of the maximum voluntary contraction (MVC) force. The single MU depicted in this example tends to discharge once every tremor-period (i.e., 125 ms in case of 8 Hz tremor); however, it also occasionally exhibits double discharges during the tremor-period.

Figure 17 depicts the simulated EMG for the three different levels of inertial loading during tremor. Without the external load, the EMG activity comprises only the phasic bursts related to tremor. Increasing the external loading increases the level of background EMG activity. At the 20% of MVC, which can be considered a relatively high contraction level with respect to the general level of muscle activity during the tasks of every day life, the background EMG activity largely masks the bursts related to tremor.

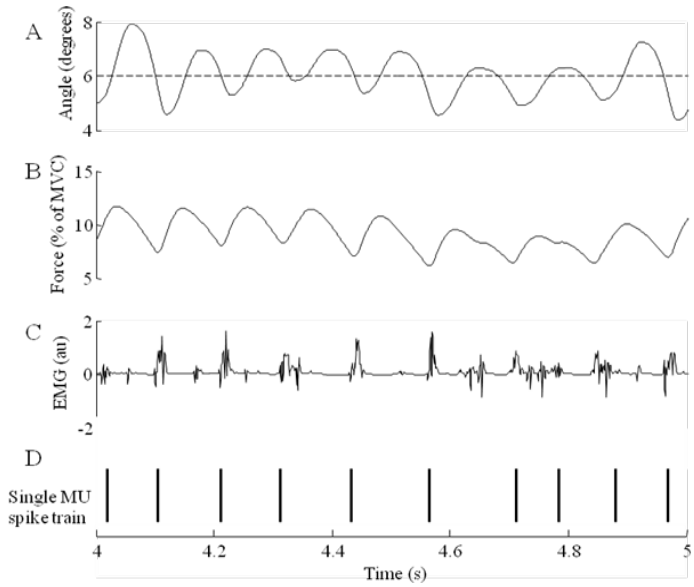

Figure 16. Representative simulation outputs. Sustained abduction of 6 degrees (voluntary movement) with 8-Hz tremor was simulated. The desired voluntary movement (A, dashed line), generated angle (A, continuous line), generated force (B), agonist EMG (C) and single MU spike train (D) are shown. The simulated EMG comprises mainly the phasic tremorogenic bursts. The isolated MU tends to discharge once in each tremor period. The oscillations of the generated angle and muscle force represent induced tremor.

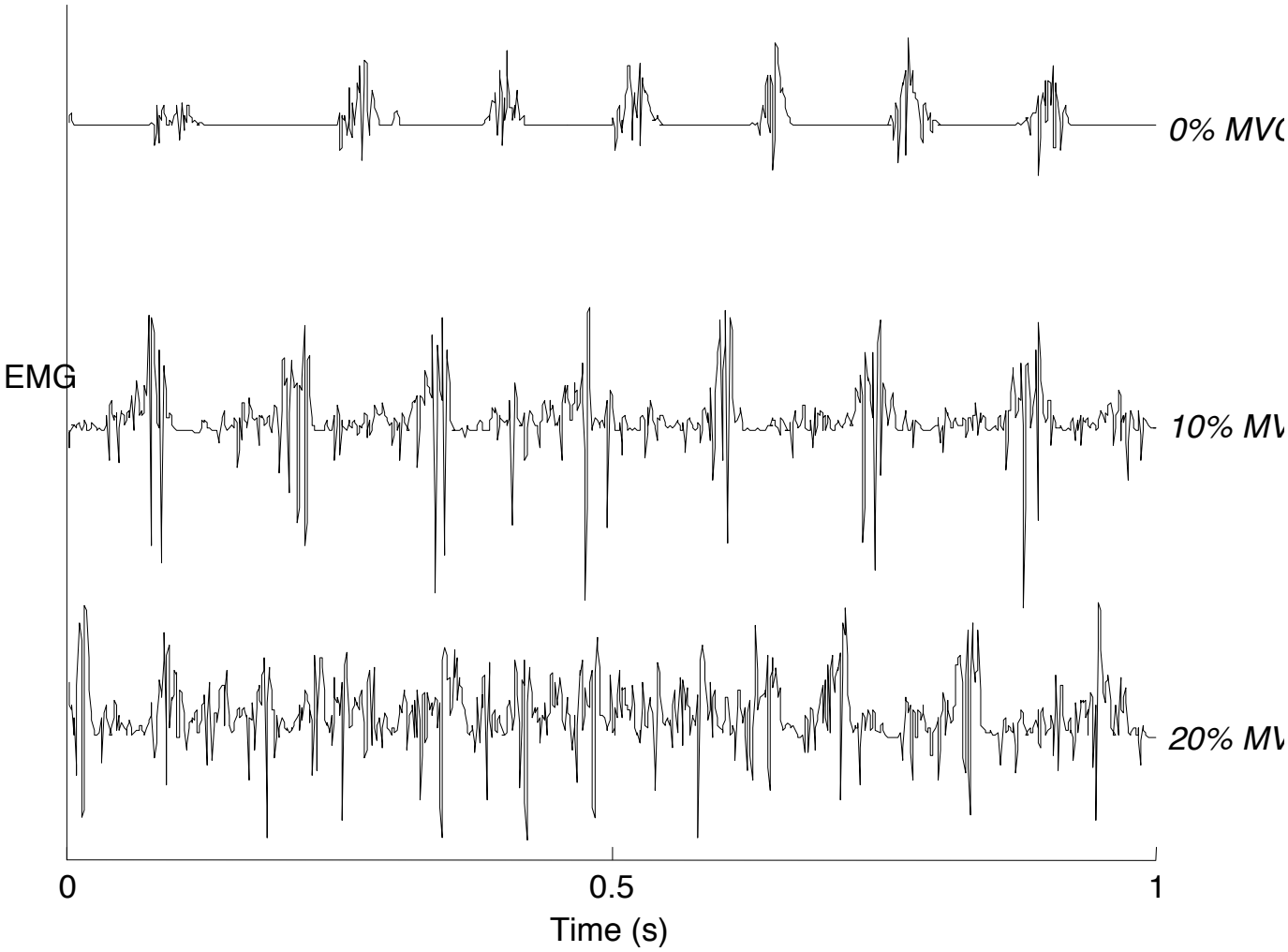

Figure 17. The simulated surface EMG for the three different levels of inertial loading during tremor. At 0% MVC, the phasic tremorogenic bursts are clearly visible. Higher loading increases the voluntary component of the EMG, gradually masking the tremorogenic activity.

3.1.2. Conclusions

A computational model able to simulate the limb angle, muscle force and surface EMG in various conditions of tremor and voluntary activation was developed. The model contains a number of sub-models, each representing relevant physiological elements of the motor system, most of which were based on the previously published and validated models. On this grounds, and based on the similarities between the characteristics of the simulation results and experimental observations, the model is regarded as a valid tool for providing surface EMG signals during tremor.

3.2. EMG-based tremor detection algorithm

3.2.1. Iterated Hilbert Transform

Iterated Hilbert Transform (IHT) is a novel multi-component decomposition method developed by Gianfelici et al., [37]. Compared to similar methods, the novel method is both computationally efficient and in most cases more effective, and this makes it an ideal choice for real-time applications. The IHT shows better demodulation performances then Hilbert-Huang Transform developed at NASA by N. E. Huang [23], Multiband Energy Separation Algorithm developed at Harvard University by P. Maragos [24], and PASED developed by B. Santhanam [25]. The IHT allows an asymptotically exact reconstruction of nonstationary biomedical signals, regardless of their duration and without any limitation in the modeling. The method permits a multi-component AM–FM model to be derived in which the number of components (iterations) may be arbitrarily chosen. Additionally, the instantaneous frequencies of these components can be calculated with a given accuracy by segmenting the phase signals. The determined multi-component model of the signal $x(t)$ has the following form:

$$\tilde{x}(t) = \sum_{i=1}^{N} a_i(t) \cdot \cos(\omega_i(t) + \varphi_i(t))$$

where $\tilde{x}(t)$ is the multi-component approximation of the original signal $x(t)$, N is the number of components, a_i is the amplitude, ω_i is the center frequency and φ_i is the instantaneous phase of the i-th component.

The IHT algorithm is summarized in Figure 18 and explained in detail in Gianfelici *et al.* [22]. It starts by calculating the Hilbert transform $H[x(t)]$ of the signal $x(t)$. The signal and its Hilbert transform are used to construct a Gabor analytic signal $z(t)$. The amplitude and phase of the Gabor signal are determined as $a_0(t) = |z(t)|$ and $\alpha_0(t) = \arg[z(t)]$, respectively. The amplitude $a_0(t)$ is separated into a trend $\bar{a}_0(t)$ and a zero-mean oscillatory component $\tilde{a}_0(t)$ by means of a suitable filtering algorithm (application dependent). The trend $\bar{a}_0(t)$ is regarded as the output of the algorithm, i.e., the first AM component, while the oscillatory part $\tilde{a}_0(t)$ is decomposed further by repeating the aforementioned steps.

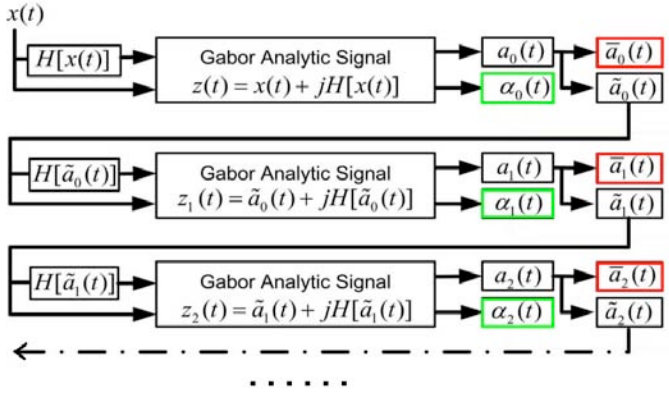

Figure 18. Iterated Hilbert Transform. Hilbert transform $H[\widetilde{a}_i(t)]$ is used to construct a Gabor analytic signal $z_{i+1}(t)$, and its amplitude $a_{i+1}(t)$ and phase $\alpha_{i+1}(t)$ are determined. The amplitude is separated into a trend $\overline{a}_{i+1}(t)$ and a zero-mean oscillatory component $\widetilde{a}_{i+1}(t)$, which is further decomposed. The outputs of the algorithm are the AM-components $\overline{a}_i(t)$ (red boxes) and phases $\alpha_i(t)$ (green boxes). The picture is adapted with permission from [37].

3.2.2. Iterated Hilbert Transform for tremor detection

The IHT was used to construct a multi-component AM-FM representation of the rectified EMG signal. By using our surface EMG model, we conducted a number of preliminary simulations in which we analyzed the spectral characteristics of the obtained AM components. Specifically, we were looking into the spectral energy around the frequency of the imposed cortical oscillations (i.e., the frequency of the imposed tremor, see Figure 15). We discovered that the energy of the first component in this band was several magnitudes higher than the energy of the other extracted components, consistently in all simulated conditions, and this indicated that the first component could be used to extract the underlying tremor signal.

Therefore, to get an estimate of the tremor, the first component extracted by the IHT is band-pass filtered within the tremor-frequency range (3-15 Hz). We also discovered that the low-passed (< 3 Hz) version of the first component gives the mean value of the rectified EMG. Therefore, to get an estimate for the level of voluntary activity, the standard deviation is calculated for the estimated tremor signal and subtracted from the mean of the rectified EMG. In this way, both the tremor component and the degree of voluntary activation can be determined from the first IHT component. This is thanks to the joint action of the heterodyning capturing effect of the Hilbert Transform and the component separation obtained by the Bedrosian Theorem.

A manuscript describing this approach is under preparation for submission to IEEE Transactions on Neural Systems and Rehabilitation Engineering, and the method has been preliminary presented at the ISEK conference, [41].

3.2.3. Validation

Methods

The validation of the method was performed in two ways:

1. First, the IHT was applied to simulated EMG data obtained by the developed model of surface EMG during tremor. Using the model has the advantage that the tremor control signal (the cortical oscillations imposed on the voluntary drive, see Figure 15) is known and can be used directly for comparison and evaluation of the output of the algorithm. Furthermore, a wide variety of conditions could be simulated in the model. Five different tremor-frequencies (4, 6, 8, 10, and 12 Hz), five different tremor-intensities (0 – no tremor, 5, 10, 15, and 20 au – severe tremor), four different degrees of voluntary activation, obtained by different inertial loadings (0, 5, 10, and 20% MVC) were simulated for 8 s contractions. Furthermore, for each of these conditions 10 simulations were performed with the varying locations of the muscle fibers belonging to each MU in the muscle. This variability is known to have a significant influence on the surface EMG, [42]. In total, this yielded 1000 simulations equivalent to 8000 s of the simulated tremor EMG. The IHT was applied to the simulated signals and compared to the imposed tremor intensity and frequency, and the degree of voluntary activity.
2. Second, the surface EMG and limb movement recorded using gyroscopes were acquired from four tremor-patients with Essential Tremor (n=2) and Parkinson's disease (n=2). The patients were instructed to perform a specific motor task provoking tremor. The task was individually selected for each patient, depending on his/her tremor type. The IHT was applied to the surface EMG signals and compared to the gyroscope recordings using the cross-correlation analysis. Furthermore, one patient was asked to repeat the task twice with 500 g and 1000 g of inertial loading, in order to assess the ability of the model to predict voluntary activation in experimental conditions.

Results

Figure 19 depicts an example of a simulated EMG signal during moderate to high voluntary activation and with 8 Hz tremor. The plot B depicts the first derived IHT-component (continuous line) compared to the imposed cortical

oscillations (dashed line). The time shift between the two signals is due to the fact that the MU action potentials tend to occur mainly during the increasing phase of the cortical oscillations. This time-shift was taken into account when systematically quantifying the similarity between the two signals. The two bottom plots depict the second and third IHT-component, which reflect the higher frequency content of the EMG. In the case of 8 Hz tremor, the mean normalized RMSE between the two signals across all simulated conditions was 18%, which indicates a high similarity.

Figure 20 depicts the correlation between the estimated and imposed tremor amplitude (A, R2=0.52) and the correlation between the estimated degree of voluntary activation and the inertial loading (B, R2=0.64) for the simulated signals. This indicates that the proposed method was capable of estimating the tremor amplitude and the degree of voluntary activation across different conditions, including the conditions with low signal-to-noise ratio (i.e., low tremor amplitude and high voluntary activation).

The influence of the length of the time-window was investigated on the simulated data. These tests indicated that the duration of the time-window had only a little influence on the estimation results, except for the window-lengths at or below 250 ms, where the peak-frequency estimation started being compromised.

Figure 21, right column depicts the tremor-estimate and the gyroscope signal for short epochs of the experimentally recorded data for each of the four patients. The left column depicts the power spectral density of these signals. The peak cross correlation value was 0.62±0.15 and the average time-lag was 13 ms, indicating the electromechanical delay.

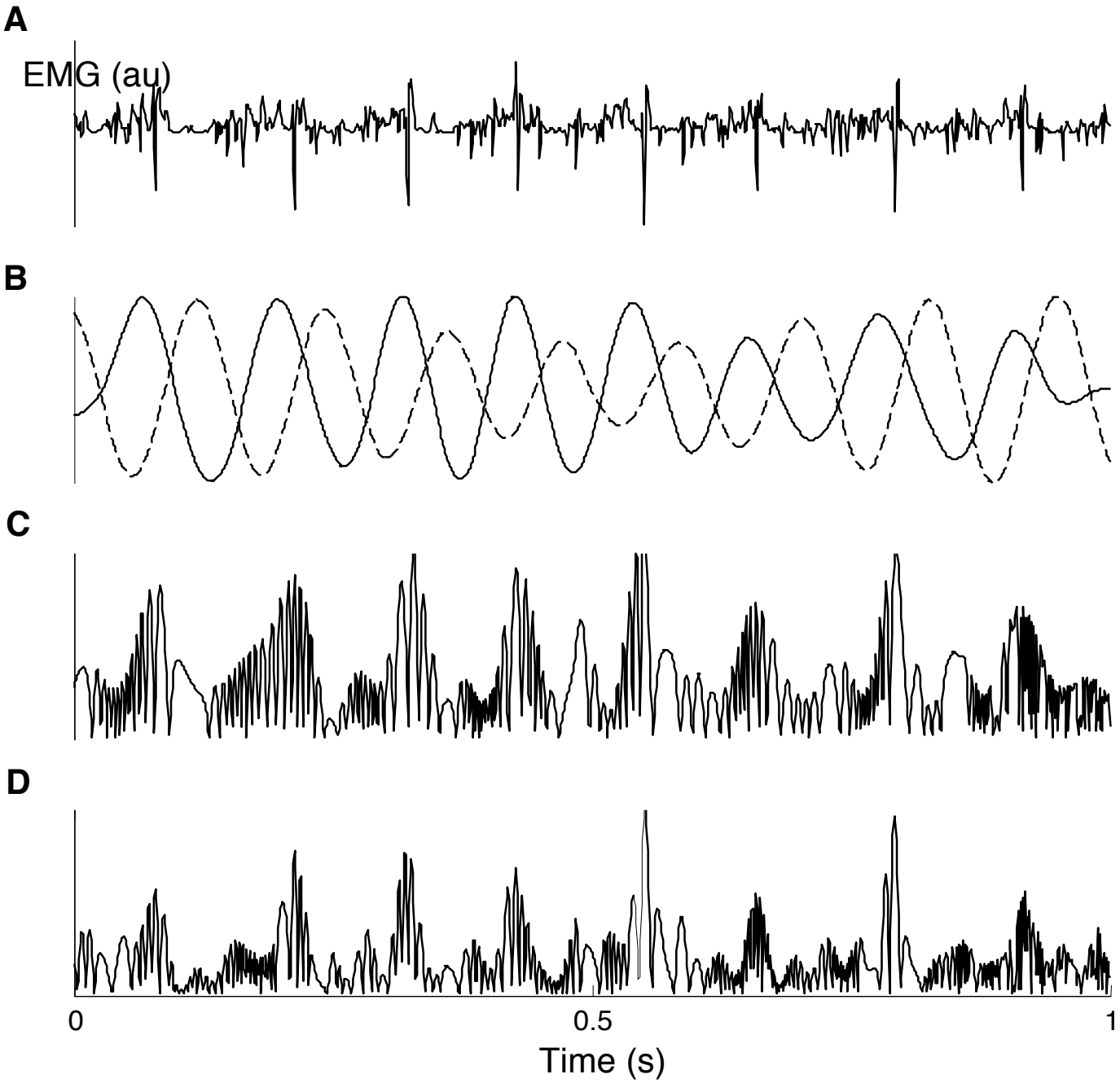

Figure 19. Algorithm performance on the simulated data during moderate levels of voluntary activity. Simulated EMG (A), imposed tremorogenic oscillations (B, dashed line), extracted tremor-component (B, continuous line) and second and third IHT-components (C and D) are shown. The estimate of the tremor signal is obtained by band-pass filtering the first component of the IHT. Note that the extracted tremor component is roughly a time-shifted version of the imposed tremorogenic oscillations.

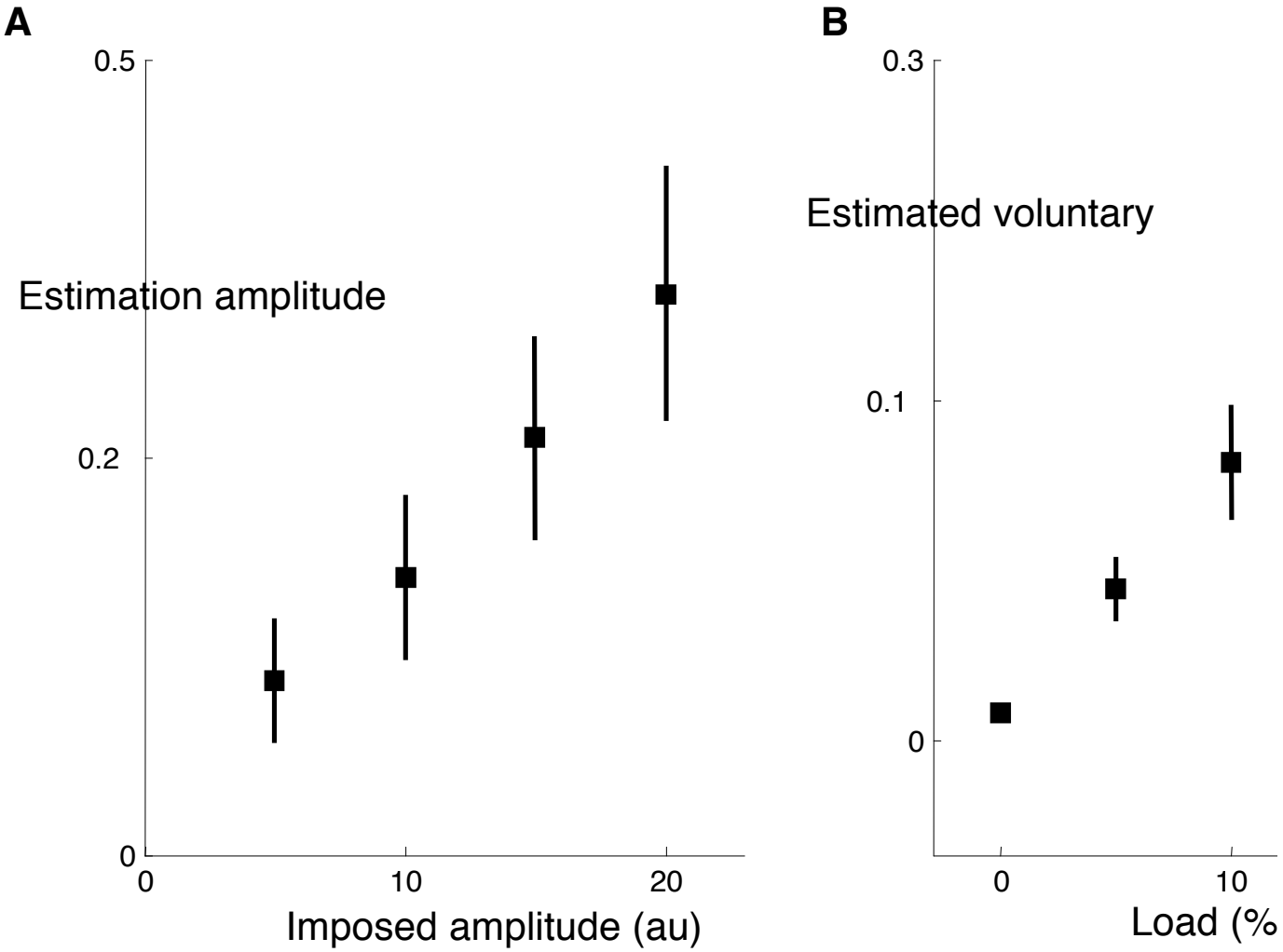

Figure 20. (A) The mean amplitude of the estimated tremor-component across all of the simulated conditions related to the amplitude of the imposed cortical oscillations and (B) The mean level of estimated voluntary activity related to the simulated added inertial loading. The IHT-based tremor detection method successfully estimates both the tremor amplitude and the level of voluntary activation.

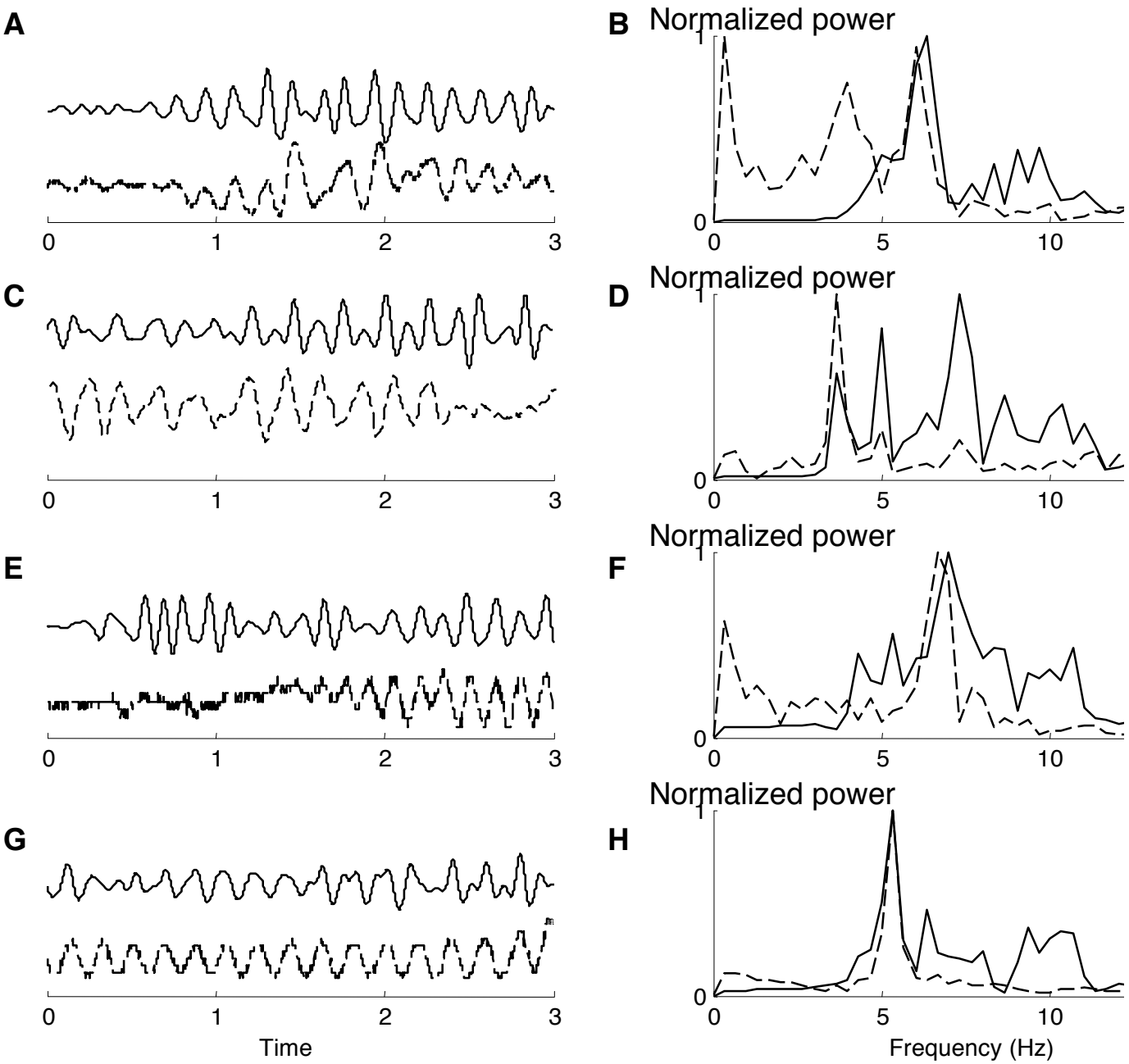

Figure 21. The tremor-estimate (full line) and the gyroscope recordings (dashed line) for the four patients (A, C, E, G) and the power spectral densities of those signals (B, D, F, H). The tremor signal estimated by the IHT resembles the actual tremor picked up by the gyroscopes, both in time and spectral characteristics.

3.2.4. Discussion

The validation of the proposed IHT-based method indicated that the method works well in characterizing tremor from the surface EMG across conditions, both on simulated and experimentally collected data.

In order to detect tremor a simple threshold can be applied to the amplitude of the extracted tremor-component. Due to interpersonal differences (e.g., muscle architecture and thickness of tissue layer between muscle and electrode) and specifics of the different detection systems (e.g., electrode impedance), the optimal performance of the tremor detection will be obtained if the threshold-value is determined individually for each subject.

Furthermore, the algorithm output may be applied in the other aspects of the tremor-suppression system: For example, the extracted tremor-component captures information about tremor-frequency and phase, which may be used as a supplement to the parameters extracted by using inertial sensors. Furthermore, the estimation of the degree of voluntary activity may be used to assess whether the voluntary movement is occurring. This is relevant

if the "stimulate-when-needed" strategy is used, i.e., the stimulation is applied only when the voluntary movement is being performed.

3.2.5. Implementation

As already pointed out, the IHT is very convenient for real time implementation. The algorithm comprises iterative application of Hilbert transformation and simple filtering. Importantly, the discrete time analytic signal can be calculated efficiently by utilizing the algorithms for the Fast Fourier transformation, [43].

To test the online performances preliminary, we implemented the IHT method in C# (Visual Studio 2005, Microsoft, US). The hardware setup comprised: 1) a single channel isolated EMG amplifier (EX002, Center for Sensory Motor Interaction, DK), 2) an accelerometer (ADXL203, Analog Instruments, US), and 3) a standard PC equipped with a DAQ card (PCI-6221, National Instruments, US). The outputs from the accelerometer and EMG amplifier were connected to the analog input channels of the DAQ card. To simulate tremor, a healthy subject was asked to generate oscillatory movement (flexion/extension) at the wrist joint. The accelerometer was placed on the subject's hand (dorsal side) to capture the oscillations, and the bipolar EMG was recorded from the wrist extensor muscles.

The signals were sampled at 1 KHz and acquired continuously. The acquired EMG was processed by applying the IHT-based tremor detection algorithm to non-overlapping time windows. Two durations of the time window were tested: 500 ms and 1s. The accelerometer signal, EMG and the extracted tremor signal (i.e., filtered first component of the IHT) were plotted (see Figure 22).

The software also calculated the average processing time (APT) for the IHT. The APT was 160 ms for the time window of 1 s. If the window of 500 ms was used, the processing time dropped to only 50 ms. The conclusion of this preliminary test is that the real time performances of the algorithm are more then adequate for the intended application. We are currently working on the implementation of the algorithm in C++ and its integration into the QNX TREMOR platform. This should improve the online performances even further.

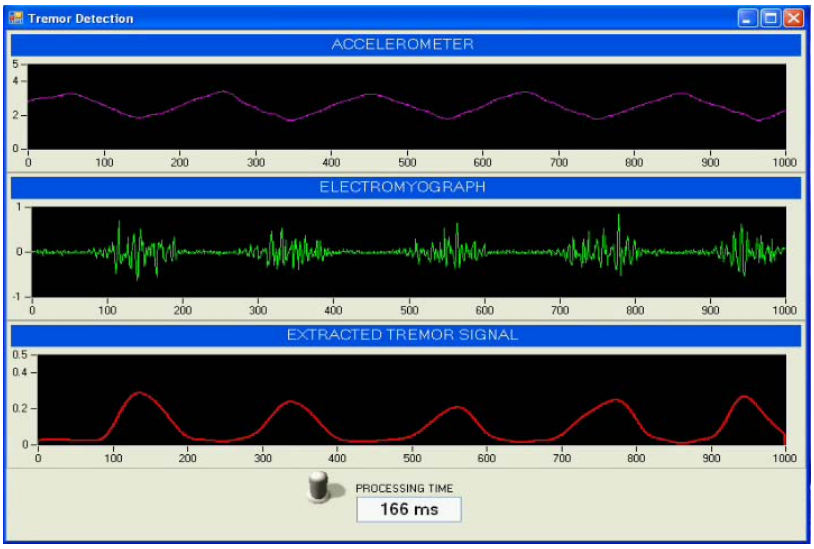

Figure 22. Online implementation of the Iterated Hilbert Transform (IHT) based algorithm for tremor detection. The method was implemented in C# in order to assess its online performances. The application acquires a signal from an accelerometer placed on the dorsal side of the subject's hand and EMG from the wrist extensor muscles and then processes the EMG by applying the IHT. The extracted tremor signal is shown in the bottom plot. The horizontal axis represents the time in milliseconds, while the vertical axes are in volts (top and middle plots) and in au (arbitrary units) for the bottom plot. The average processing time for the time window of 1 s of EMG was about 160 ms.

4. Development of inertial sensor subsystem

In the context of this task, CSIC and TCN led the definition of the Inertial Sensor Subsystem to be used in TREMOR. The inertial system is a new generation of IMUs based on off-the-shelf Technaid IMUs, developed by taking into account the results of the preliminary recording session held at Hôpital Erasme. IMUs are used within TREMOR to:

1) Work out limb posture (as a source of information for WP5),

2) Extract tremor parameters at joint level. In particular, for the first objective of the IMU system is the definition of a body to sensor calibration protocol in order to translate the recorded motion with IMU into joint rotations. This procedure permits fast sensor placement and robustness when there is uncertainty in sensor placement, as it might appear when the user is wearing the final garment. The analysis of the upper body motion based on inertial sensors will be described in section 4.1.

TCN customized its IMU product for TREMOR project. The sensor eventually developed is able to provide information about joint acceleration, velocity and position, Figure 23. Moreover, a biomechanical model for the extraction of this information based on IMUs sensors was developed. TCN also developed a QNX Neutrino driver for the integration of IMU sensors in the TREMOR platform.

Figure 23. Technaid's inertial sensor customized for TREMOR project.

Technaid started the development of flexible IMU sensors in the framework of TREMOR, Figure 24. The major benefits of these sensors are: (1) they can be easily integrated into TREMOR garment (can adapt to human shape), (2) they have reduced weight and size (lower thickness), and (3) they increase patient comfort when wearing the garment, in addition to improving their esthetical acceptance. Currently, Technaid has developed flexible circuits composed only by gyroscopes. The developed sensors were sent to ULB in order to assess tremor in rats. Based on the result of these experiments, Technaid will start to develop complete inertial sensors in flexible form.

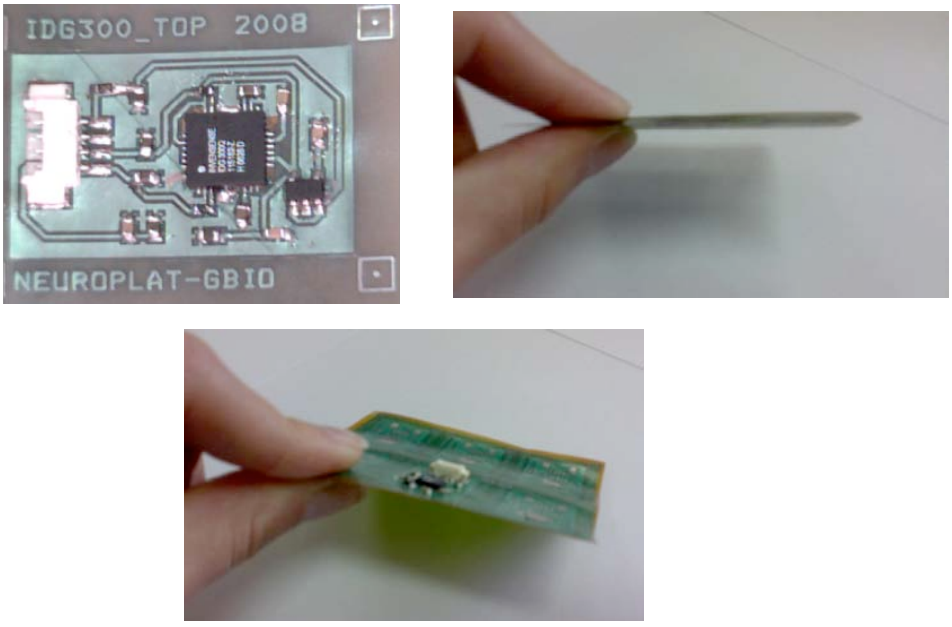

Figure 24. Flexible IMU sensors developed by Technaid to be integrated into TREMOR garment.

4.1. Analysis of the upper body motion using inertial sensors

The kinematic model of the arm can be built based on a kinematic chain based on the orientation and lengths of the body segments. In Figure 25, the upper arm is represented. p_{U0} is the position of the shoulder and p_{u1} is the position of the elbow. The position of the elbow can be calculated from the position of the shoulder using the following equation (assuming a rigid segment):

$$^{G}p_{U1} = {}^{G}p_{U0} + {}^{GB}q_{U} \otimes {}^{B}s_{U} \otimes {}^{GB}q_{U}^{*} \quad \text{(Elbow coordinates)}$$

Where:

$^{G}\mathbf{p}_{U1}$ = position of the elbow respect to the global frame.

$^{G}\mathbf{p}_{U0}$ = position of the shoulder respect to the global frame.

$^{GB}\mathbf{q}_{U}$ = orientation of the upper arm represented by quaternions.

$^{B}\mathbf{s}_{U}$ = length of the upper arm.

$^{GB}\mathbf{q}_{U}^{*}$ = conjugate of the quaternion $^{GB}q_{U}$.

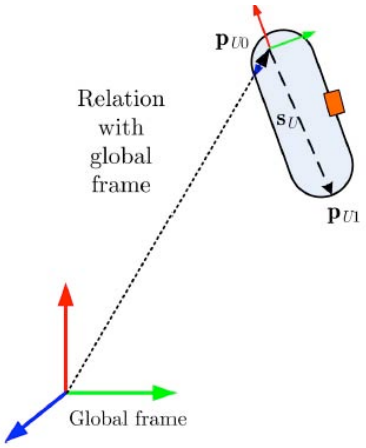

Figure 25. Body segment frame respect to the global frame.

The position of the wrist can be calculated from the position of the elbow using the following equation:

$$^{G}p_{F1} = {}^{G}p_{U1} + {}^{GB}q_{F} \otimes {}^{B}s_{F} \otimes {}^{GB}q_{F}^{*}$$

Therefore, a joint is calculated from the previous joint. In TREMOR's case, for the kinematic model of the upper body the first join could be the pelvis. According to these considerations the kinematic model consists of the following equations:

$^{G}\mathbf{p}_{pelvis}$ = Origin — Pelvis

$$^{G}p_{L5} = {}^{G}p_{pelvis} + {}^{GB}q_{L5} \otimes {}^{B}s_{L5} \otimes {}^{GB}q_{L5}^{*}$$ — L5

$$^{G}p_{L3} = {}^{G}p_{L5} + {}^{GB}q_{L3} \otimes {}^{B}s_{L3} \otimes {}^{GB}q_{L3}^{*}$$ — L3

$$^{G}p_{T2} = {}^{G}p_{L3} + {}^{GB}q_{T2} \otimes {}^{B}s_{T2} \otimes {}^{GB}q_{T2}^{*}$$ — T2

$$^{G}p_{T8} = {}^{G}p_{T2} + {}^{GB}q_{T8} \otimes {}^{B}s_{T8} \otimes {}^{GB}q_{T8}^{*}$$ — T8

$$^{G}p_{shoukder} = {}^{G}p_{T8} + {}^{GB}q_{shoulder} \otimes {}^{B}s_{shoulder} \otimes {}^{GB}q_{shoulder}^{*}$$ — Shoulder

$$^{G}p_{elbow} = {}^{G}p_{shoulder} + {}^{GB}q_{Upperarm} \otimes {}^{B}s_{Upperarm} \otimes {}^{GB}q_{upperarm}^{*}$$ — Elbow

$$^{G}p_{wrist} = {}^{G}p_{elbow} + {}^{GB}q_{forearm} \otimes {}^{B}s_{forearm} \otimes {}^{GB}q_{forearm}^{*}$$ — Wrist

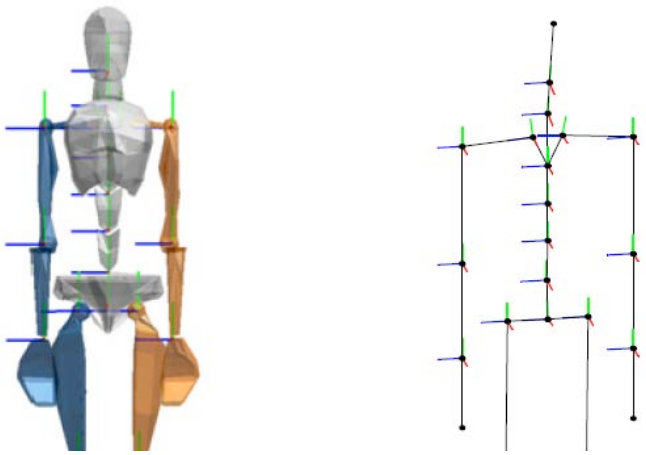

Figure 26. Reference frames for the joints.

As result, the analysis of the upper body motion is reduced to know the orientation of each body segment respect to the global frame, so that, the quaternion of each body segment. These orientations are obtained from the inertial sensors placed on the different segments of the body, figure 26.

4.1.1. Measurement of the body segment orientation using inertial sensors

The inertial sensors provided by Technaid integrate a three-dimensional accelerometer, a three-dimensional gyroscope and a three-dimensional magnetometer. The information of these three sensors is combined in order to estimate the orientation of the segment where the sensor is attached. The orientation of a vector can be also calculated using the angular velocity of its motion by the equation:

$$^{GS}{}_{o}q_{t} = \frac{1}{2}\,{}^{GS}q_{t}\,x\,\Omega_{t}$$

That means that the orientation of the body limb could be calculated by the gyroscope signals. Therefore, the orientation of the body limb can be estimated combining the accelerometer, gyroscope and magnetometer and only from the gyroscope signals. This redundant information can be used to improve the robustness of the system.

Each sensor offers the orientation of the body limb where it is attached. Based on these orientations and the kinematic model, the upper body motion can be rebuilt. However, the orientation given by the sensor is referred to the global frame and the orientation of the sensor respect to the body segment is unknown. Therefore, it is necessary a calibration process in order to know the position of the sensor respect to the body segment.

The body orientation respect to the global frame (^{GB}q) can be calculated following equation:

Where,

- ^{GS}q is given by the sensor,
- ^{BS}q is estimated after calibration process,
- ^{GB}q is the quaternion representation of the body segment orientation respect to the global frame,
- ^{BS}q is the quaternion representation of the sensor orientation respect to the body frame,
- ^{GS}q is the quaternion representation of the sensor orientation respect to the global frame (measurement of the sensor).

Therefore, the calibration process is carried out in order to know the orientation and position between the sensor and the body limb. The process defined by Technaid consists of three steps or poses.

N-pose

- Stand upright on a horizontal surface
- Feet parallel, one foot width apart
- Knees above feet
- Hips above knees

- Back straight
- Shoulders above hips, do not pull shoulders up.
- Arm straight alongside body (vertically), thumbs forwards. Check the correct attitude of the arms by flexing and extending the elbows. The forearms should move only in the vertical (sagittal) plane with the palms of the hands facing each other.
- Face forward.
- Do not move during the calibration procedure.

T-pose

- Stand upright on a horizontal surface
- Feet parallel, one foot width apart
- Knees above feet
- Hips above knees
- Back straight
- Shoulders above hips, do not pull shoulders up.
- Arms extended horizontally, thumbs forwards. Check the correct attitude of the arms by flexing and extending the elbows. The forearms should move in horizontal (transverse) plane.
- Face forward.
- Pay attention to symmetry, for example, keep the arms at an equal height.
- Do not overextended the elbow, since flexion/extension may be projected in other axes.
- The wrists, elbows and shoulders should all be on a single line.

Hand touch

- Place the palms of the hands together
- Move the arms around slowly while keeping the hands together and shoulders steady.
- Make small circles in all directions.

With the N-pose the misalignment between the global vertical axis and the sensor axis parallel to the limb (Y axis) is calculated. The global vertical direction is the gravity. With the T-pose, the misalignment between the global vertical axis and the sensor axis perpendicular to the body limb (X axis) is calculated. With the Hand touch step both arms are as a close chain, which allows calculating the lengths of the limbs.

With the following expression, the orientation between the sensor and the body limb can be calculated ${}^{GB}q$ is the orientation of the global vertical axis or gravity vector and ${}^{GS}q$ is the measurement):

5. Development of algorithms for tracking and extraction of tremor characteristics

This section summarizes work on task WP4.4 Development of algorithms for tracking and extraction of tremor characteristics, which aims at obtaining an instantaneous parameterization of tremor in each targeted joint.

This task is coordinated by CSIC, and interacted with TCN for the development and validation of the tremor tracking algorithms. Notice that the work described hereafter has been included in a number of peer-reviewed publications, among them, [44, 45].

The work was organized as follows:

- Propose a preliminary algorithm for extraction of tremor characteristics based on data collected form tremor patients.

- Validation and refinement of this algorithm In subsequent recording sessions.

- Update the different parameters of the algorithm for the customized IMUs.

Data presented here was obtained from five patients recorded during the first session at Hôpital Erasme, Brussels. Similar results for all upper limb joints have been obtained in subsequent experiments. The group of patients comprised essential tremor patients (n=2), a paraneoplastic syndrome patient, an idiopathic parkinsonian patient, and a patient suffering from extrapyramidal syndrome. This group comprised 4 men and 1 woman, with ages ranging from 48 to 73 years old (mean=64). All the patients gave written informed consent, and the protocol had been previously approved by the Ethical Committee at Hôptial Erasme. Patients kept taking their medication during the experiments, so that their tremor were stabilized. The description of the patients were given in section 2.

Protocol

We present wrist flexion/extension data because: 1) tremors are more explicit at distal joints, [56], 2) wrist tremor has the largest impact on disability, [65], and 3) it constitutes, together with finger tremor, the most studied tremor in clinical literature.

The protocol comprised four tasks, three of them included because there are commonplace in clinical practice, the last one for usability analysis. These tasks are: 1) resting both arms on the lap, 2) keeping both arms outstretched, 3) pointing with the finger tip to the nose, the so called finger to nose test, and 4) pouring water from a standard bottle into a regular glass.

Each patient performed three repetitions of each task, each lasting 30 s. The finger to nose test was executed with both hands.

Instrumentation

Joint rotation is obtained with two solid state gyroscopes included within the IMU, placed distally and proximally with respect to the human joint. Figure 27 shows how wrist flexion/extension is obtained: we remove the measurement of the distal gyroscope, placed over the dorsal side of the hand, from the measurement of the proximal gyroscope, placed over the dorsal side of the forearm. Fixation on soft tissues is avoided in order to eliminate the undesired oscillations they create, and their intrinsic low pass filtering behaviour, [52].

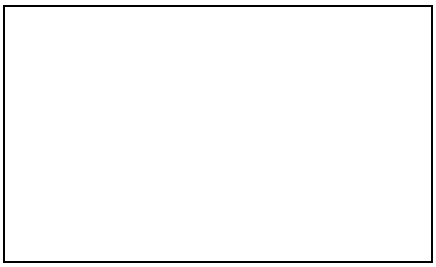

Figure 27. Placement of MEMS gyroscopes (red boxes) for recording wrist flexion/extension. Differential measurement directly provides wrist rotation.

Gyroscope bias is compensated online, based on its correlation with temperature, which is measured by the IMU itself. Correlation between gyroscope bias and temperature in three axes of one of the inertial measurement units (IMUs) we employ is shown in Figure 28. Regression coefficients for the three gyroscopes in one of the chipsets are given in Equations (1) to (3), where b_{axis} represents the bias for each axis, and T the temperature in °C.

(1)

(2)

(3)

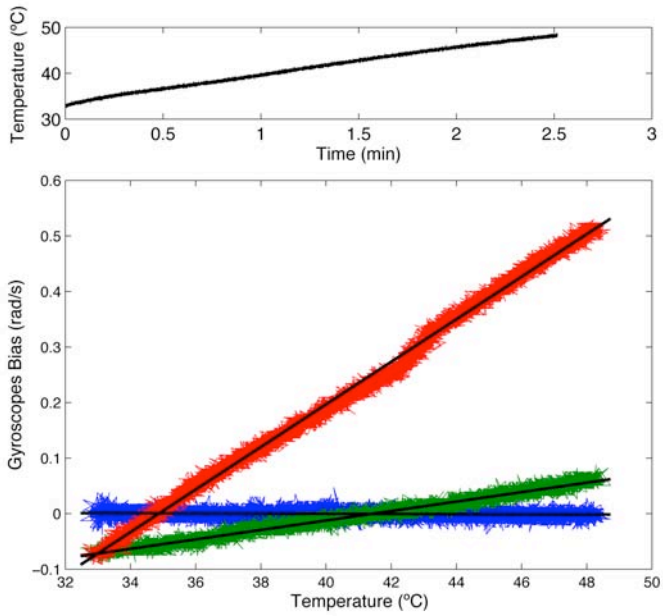

Figure 28. Relationship between gyroscope offset and temperature. Top plot shows temperature variation measured by the IMU. Bottom plot shows correlation between offset and temperature for X (blue), Y (green) and Z (red) axis gyroscopes. High correlation is observed.

5.1. Real-time estimation of instantaneous tremor parameters

Most of currently existing tremor estimation algorithms have been developed for cancelling physiological tremor in human-machine interfaces. Physiological tremor has another aetiology than pathological tremors, and possesses also different characteristics: it is barely visible to the unaided eye, and has frequency between 8 and 12 Hz, [46]. Physiological tremor is only symptomatic during high precision tasks, thus it is typically employed during hand held surgery. According to this, successful algorithms for cancelling physiological tremors such as the classical Weighted frequency Fourier Linear Combiner (WFLC), [47], Bandlimited Multiple Fourier Linear Combiner (BMFLC), [48], or Double adaptive BMFLC, [49], may not constitute the optimal solution for estimation of pathological tremor parameters. In fact, in [50], Rocon and colleagues employ a preliminary filtering stage that eliminated volitional motion from the input signal before feeding it into a WFLC, which was employed to track pathological tremor. A similar approach has been recently described in [51]: an extended Kalman filter separates tremor and the concomitant voluntary component of movement, and estimates tremor features.

This section presents our two-stage algorithm for real-time modelling of tremor. It relies on two assumptions: 1) pathological tremors and voluntary motions have different frequency distributions, and 2) pathological tremor constitutes, from a signal processing standpoint, additive noise superimposed to volitional movement, [53].

The data we collected yields that pathological tremors occur in a frequency band higher than voluntary motion, Figure 29, which is in agreement with the literature. For example, one large study carried out with young and elderly healthy people and patients suffering from tremor, demonstrates that both groups are able to perform tracking tasks with a frequency up to 2 Hz, the bandwidth decreasing with age, [54]. Also in [55], the authors perform a large spectral analysis of twenty four activities of daily living, showing that most of them involve wrist notion in a frequency range around 1 Hz, being the predominant frequency components between 0.48 and 2.47 Hz.

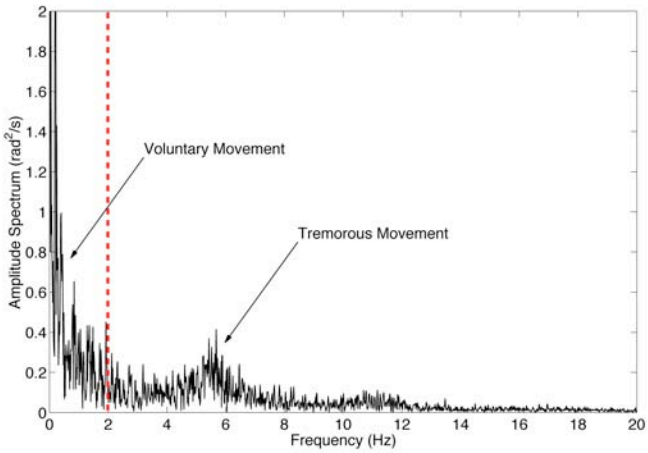

Figure 29. Power spectral density of wrist rotation during a finger to nose task performed by an essential tremor patient. Voluntary movement (below 2 Hz) has considerably more energy than tremorous movement (centered around 5.5 Hz). Dashed red line separates energy attributed to voluntary (left) and tremorous motion (right).

In addition, pathological tremors are reported to occur at higher frequencies, typically in the 3–12 Hz band, [56,57]. Moreover, there exists a relationship between the underlying pathology and tremor frequency. For example, Parkinsonian tremor frequency lies within 4–7 Hz, cerebellar tremors manifest between 4 and 6 Hz, and essential tremors broaden to basically the whole 3–12 Hz band, [56].

According to this, it is possible to extract voluntary and/or tremorous motion from kinematic data time series based solely on their different frequency contents, for example with a forth and back recursive digital filter that removes one of them from the original signal without causing phase distortion, i.e., delay, Figure 30. Although this approach is not real-time implementable, it sets the basis for our two-stage algorithm for estimation of tremor parameters described in next section.

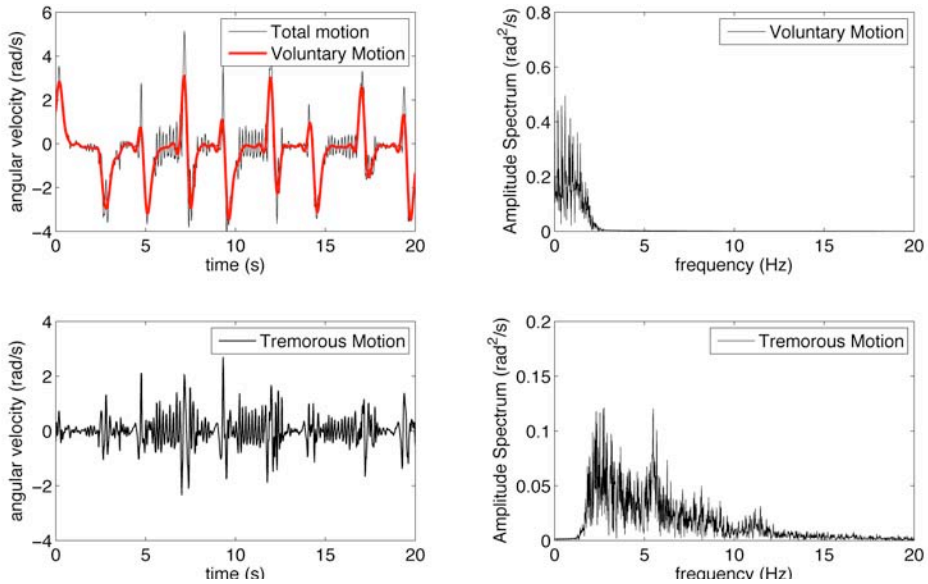

Figure 30: Separation of voluntary and tremorous components of movement by means of recursive digital filters. Top left figure shows the original signal (black) and voluntary movement (red) obtained with a zero phase low pass filter, f_c = 2 Hz. Bottom left plot shows tremorous movement obtained by subtracting voluntary movement from the original signal. Right plots show power spectral densities of voluntary (top) and tremorous components (bottom).

However, at the moment of developing a real-time algorithm, we must take into account that power of tremorous component of motion is considerably smaller than that of volitional origin. This makes estimation algorithms based on gradient like approaches tend to converge towards the voluntary component, making them unsuitable for direct tremor modelling, [54]. Therefore, we need to first isolate the tremorous component of motion. This constitutes the idea of our two stage algorithm: to first generate an estimation of tremorous motion (after stage 1),

and next feed this signal into an adaptive algorithm that provides instantaneous tremor frequency and amplitude (stage 2), Figure 31. To generate an estimation of tremor, we employ a tracking algorithm to estimate the voluntary component of motion. Next, based on the fact that tremor alters volitional motion in an additive manner, [43], we remove the estimated voluntary movement from the input signal, obtaining an estimation of tremor.

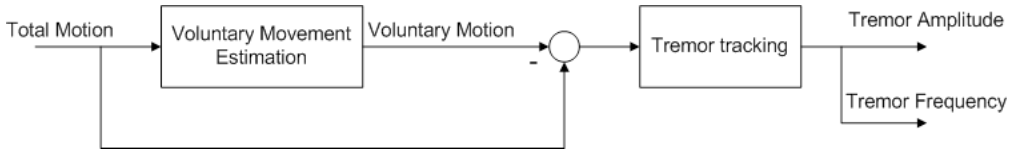

Figure 31: Block diagram of the two stage algorithm for real-time estimation of tremor parameters. First, we generate an estimation of the voluntary component of motion, which subtracted from the total movement yields an estimate of tremor. Afterwards, in stage two, and adaptive algorithm tracks instantaneous tremor parameters.

This section reviews a series of algorithms that are employed to develop the two-stage algorithm. First, we present a number of techniques to track voluntary movement based on its lower frequency content. Next, we introduce two adaptive algorithms that track an input signal based on Fourier modelling and the Least Mean Square (LMS) recursion, a gradient-like approach [58], and a Kalman Filter that estimates pathological tremor amplitude.

5.1.1. Stage 1. Voluntary motion tracking

Two types of tracking algorithms for real-time estimation of voluntary movement will be evaluated. As discussed above, voluntary movements are assumed to be performed between 0 and 2 Hz. Therefore, the tracking algorithm must be designed to neglect any component of the movement over 2 Hz.

Voluntary movement is modelled as a first order process. If we consider a Taylor series that represents voluntary movement, we can neglect the second derivative if either the sampling period T_s or the acceleration itself are small, Equation (4). In our case both assumptions are satisfied: the sampling period is 1 ms, and the maximum acceleration is $2.54 \cdot 10^{-4}$, 4 orders of magnitude smaller than average angular velocity.

(4)

g-h filters

g–h filters are simple recursive filters that estimate future position and velocity of a variable based on first order model of the process. Measurements are used to correct these predictions, minimizing the estimation error. Traditional applications of g–h filters are radar tracking and aeronautics, [59]. The general form of a g–h filter is:

(5)

(6)

(7)

(8)

Equations (5) and (6) are designated as update, tracking, or filtering equations. They estimate the current position and velocity of the variable, , , based on previous predicted position and velocity, , , taking current measurement into account. Confidence on measures is weighted by gains and . Equations (7) and (8) are called prediction equations, because they provide a prediction of the position and velocity based on the first order dynamic model of the variable. Note that as g–h trackers consider a constant velocity model, predicted velocity is equal to the current one.

g–h filters are affected by two error sources, [59]: 1) the lag, dynamic, bias or systematic error, which is related to the constant velocity assumption, and 2) the measurement error, which is inherent to the sensor and measurement process. Typically, the smaller and are, the larger is the dynamic error and the smaller are the measurement errors, [59]. Therefore, in designing a g–h tracking filter there is a degree of freedom in choice of the relative magnitude of the measurement and dynamic errors. To simplify the selection of gains, we consider

two filters that are optimal in some sense. These filters are the Benedict–Bordner Filter and the Critically Dampened filter, described next.

- Benedict-Bordner Filter (BBF): The BBF minimizes the total transient error, defined as the weighted sum of the total transient error and the variance of prediction error due to measurement noise errors, [60]. The BBF is the constant g–h filter that satisfies:

(9)

As Equation (9) relates g and h, the BBF has one degree of freedom. Because for g–h filters increasing the value of g diminishes the transient error, the larger g is, the higher frequencies the BBF tracks.

- Critically Dampened Filter (CDF): The CDF minimizes the least squares fitting line of previous measurements, [59], giving old data lesser significance when forming the total error sum. This is achieved with weight factor θ. Parameters in the g–h filter are related by:

(10)

Selection of filter gain for the CDF is analogous to that for the BBF.

Kalman Filter

The Kalman filter (KF) is the most widespread estimation algorithm, and is employed in a large number of applications. We implement a KF that tracks voluntary movement modelled as a first order process, Equation (4). Therefore, state vector $x(t)$ is composed by the variable to be estimated, and its derivative. The problem is formulated as:

(11)

(12)

Covariance matrices are defined taking into account the following considerations:

1. Measurement noise covariance $\mathbf{R}(k)$: as voluntary motion is the variable we are tracking, tremor is assumed to be sensor noise. The value of the measurement noise covariance is considered to be the average covariance of isolated tremor data; therefore = 0.0643 $rad^2 \cdot s^{-2}$.
2. Process noise covariance $\mathbf{Q}(\mathrm{k})$: we hypothesize that process noise is related to voluntary motion changes due to tremor. A piecewise constant acceleration model is considered, [JAG18]. This model assumes that voluntary movement undergoes constant and uncorrelated acceleration changes be tween samples in the form of:

(13)

To select the variance of the random velocity component, , we follow the recommendation in [61]: . The second derivative of the raw recorded motion yields that: = 0.1042 $rad^2 \cdot s^{-2}$.

5.1.2. Stage 2. Tremor modelling

State of the art tremor modelling algorithms rely on a time-varying Fourier series, which parameters are estimated recursively. Adaptation to the input signal is based on the LMS algorithm developed by Widrow, [58]. As the LMS technique is a descend method that relies on a special estimate of the gradient, [58], high energy voluntary motion must be removed first, to ensure proper tremor tracking. The first part of the two-stage algorithm accomplishes this task, Figure 31.

We evaluate the performance of two algorithms originally developed to track physiological tremor, and of a Kalman Filter we have developed to estimate tremor amplitude, the parameter that is more prone to change

during the execution of a task, while tremor frequency keeps within a 1.5 Hz interval around tremor frequency, [62].

Weighted Frequency Fourier Linear Combiner

The Weighted Frequency Fourier Linear Combiner (WFLC) is the most widespread algorithm for tremor modelling. It consists in an extension of the classical noise canceller presented in [58], the Fourier Linear Combiner, [63], which also tracks frequency of the input signal based on a LMS recursion. Therefore, the WFLC adapts in real-time its amplitude, frequency and phase, [54]:

(14)

(15)

(16)

(17)

Equation (14) represents the time varying sinusoidal terms of the Fourier Series. Equation (15) defines the error to be minimized by the LMS recursion. Equations (16) and (17) represent frequency and amplitude adaptation. The WFLC has four parameters: the number of harmonics of the model, M, the amplitude and frequency adaptation gains, μ_0, and μ_1, and a bias weight μ_b that is included to compensate for low frequency errors, [54,64]. The number of harmonics is typically set to 1; the other parameters are selected based on experimental data.

Bandlimited Multiple Fourier Linear Combiner

The Bandlimited Multiple Fourier Linear Combiner (BMFLC) is a more recent algorithm derived from the FLC. It emerged to compensate for the limitations of the WFLC to track physiological tremor when two constituent frequencies are clearly evident, [46], or when frequency variations occur abruptly, [48]. The BMFLC consists in a bank of FLCs that track the input signal based on multiple frequency components. Therefore, each FLC adapts its amplitude to the input signal, although its frequency remains constant.

The performance of the BMFLC relies on the multiple fixed frequencies it can track. An interval is thus defined with the lower and upper frequency of the FLCs bank, ω_0 , and ω_f . The number of FLCs in between is defined by parameter G. The BMFLC is formulated as follows, [48]:

(18)

(19)

(20)

Equation (18) represents the sinusoidal terms of the Fourier Series. Equation (19) defines the error to be minimized by the LMS recursion. Equation (20) represents amplitude adaptation. The BMFLC has six parameters: the number of harmonics of each FLC model, M, amplitude adaptation gain, μ, the lower and upper frequency of the FLC bank, ω_0, and ω_f , and the number of filters in between, G. A bias weight μb is also included to compensate for low frequency errors [16].

Although the BMFLC is not conceived as a frequency tracking algorithm, we developed an equation to estimate the current frequency of the input signal, Equation (21). Frequency estimation is obtained by weighting the contribution of each FLC to amplitude adaptation. For a first order Fourier series, it is expressed as:

(21)

Kalman Filter

The WFLC and BMFLC algorithms provide adaptation to the input signal based on special estimates of the gradient. On the contrary, Kalman Filter (KF) constitutes the optimal solution for estimation problems, in the sense it minimizes the covariance of a posteriori estimation error. Therefore the performance of WFLC and BMFLC, overall in terms of amplitude estimation, as it is the parameter that varies the most, can be enhanced using an adequate KF. In a similar manner to WFLC, we define our KF as:

(22)

(23)

where A and B represent the amplitude of the sinusoidal terms of a first order Fourier series, and ω_0 the current tremor frequency. As tremor frequency suffers slow changes, and varies in a ±1.5 Hz interval around a characteristic frequency that depends on the patient, [62], WFLC frequency estimation is employed. Therefore, we define a cascade filter that consists of a WFLC that tracks tremor frequency, and feds it into the Kalman Filter that estimates tremor amplitude.

Covariance matrices are adjusted as follows:

1. Measurement noise covariance , which has only slight impact on transient duration.
2. Process noise covariance is defined as , because state variables are considered to be mutually independent.

5.2. Results

This section presents evaluation of the algorithms described in previous section for both voluntary motion tracking, and estimation of tremor parameters. The idea is to find a unique filter setup that provides accurate tracking of instantaneous tremor parameters for every patient and task. To do so, first, we present the figure of merit that will be employed to tune each algorithm, and compare the performance of different candidates. Next, we summarize the results obtained with each of them.

The results presented below are obtained after analyzing wrist tremor of five patients recorded during the first session at Hôpital Erasme, Brussels. The protocol for the measurement was described in section 2.1. Similar results for all upper limb joints have been obtained in subsequent experiments. We present wrist flexion/extension data because: 1) tremors are more explicit at distal joints, [56], 2) wrist tremor has the largest impact on disability, [65], and 3) it constitutes, together with finger tremor, the most studied tremor in clinical literature.

5.2.1. Evaluation of voluntary movement tracking algorithms

The Kinematic Tracking Error (KTE) evaluates the smoothness, response time, and execution time of a tracking algorithm, [64]. It is expressed mathematically as:

(24)

where $\varphi_{|b*|}$ and $\sigma_{|b*|}$ are the mean and variance of the absolute estimation error, $b^* = |y_k - x_{k+1,k}|$, respectively. The former measures how fast the algorithm is capable of reacting when the velocity changes, whereas the latter quantifies the smoothness or filtering of the estimated variable, [64]. Offline voluntary motion estimation obtained with a forth and back recursive filter is employed as the reference signal the estimators should track. This technique consists in filtering input data in both the forward and reverse directions; after filtering in the forward direction, the algorithm reverses the filtered sequence and runs it back through the filter, which yields precisely zero-phase distortion.

First, we present results obtained with the optimal parameter(s) for each of the voluntary movement estimation algorithms presented in Section 5.1.1. The condition to select the optimal parameter(s) for each algorithm is to

find the tuning that minimizes the KTE between filter estimation of voluntary motion and zero phase (off-line) recursive estimation of voluntary movement. Optimal filters are:

- Benedict–Bordner Filter with g = 0.018.
- Critically Dampened Filter with θ = 0.990.
- Kalman Filter with [ ] = 0.0643 and [ ] = 0.1042.

The KTE is employed next to compare their relative performance. Table VI summarizes KTE per kind of task and patient, for the optimal setup for the three algorithms. We observe that among the BBF, CDF, and KF, the CDF with θ = 0.990 performs the best when tracking voluntary movement, as it provides the least KTE for all tasks; thus it is the approach we select for the first stage of the algorithm.

Algorithm	Arms outstretched	Finger to nose	Rest	Water into glass
Benedict-Bordner Filter	0.194 ± 0.058	0.400 ± 0.134	0.147 ± 0.091	0.291 ± 0.083
Critically Dampened Filter	0.121 ± 0.053	0.372 ± 0.118	0.134 ± 0.081	0.264 ± 0.073
Kalman Filter	0.169 ± 0.100	0.378 ± 0.143	0.174 ± 0.129	0.312 ± 0.124

Table VI. Kinematic Tracking Error (rad/s) for voluntary movement tracking algorithms organized by task. Table provides mean ± standard deviation.

Figure 32 shows an example of CDF and BBF estimation of voluntary movement from raw gyroscope recording, during an arms outstretched task performed by patient 01. We observe that BBF estimation is less smooth than that of the CDF for a similar adaptation to transitory changes.

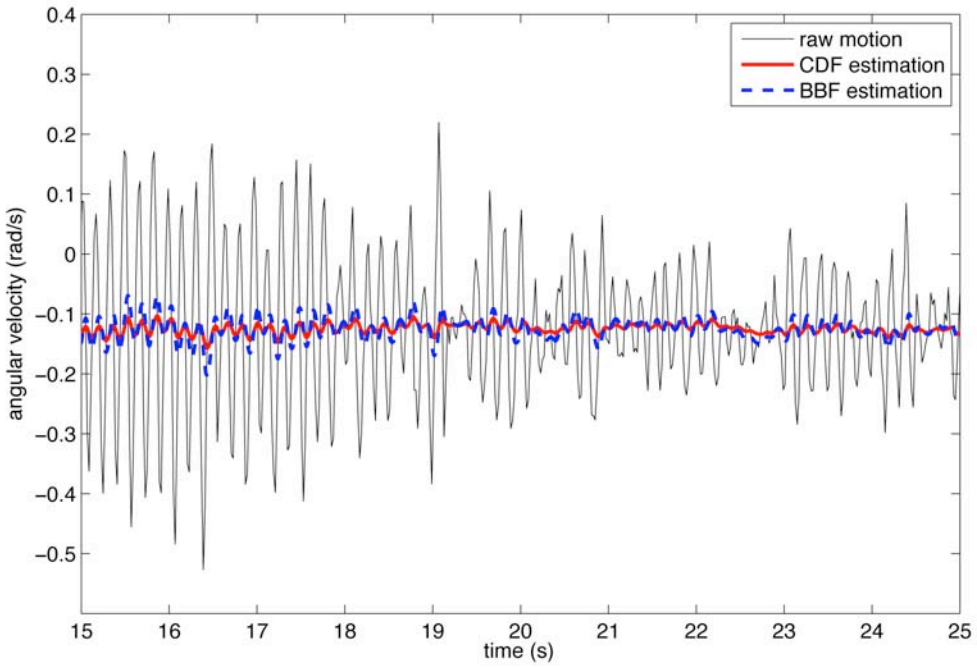

Figure 32. Comparison between CDF and BBF estimation of voluntary movement from raw gyroscope data during an arms outstretched test performed by patient 01.

5.2.2. Evaluation of tremor modelling algorithms

An optimal figure of merit to evaluate tremor estimation algorithms must consider the physical nature of the estimation error; for example if it originates from phase difference between real and estimated tremor, or estimation overshoots and undershoots. Traditional use of root mean square error (RMSE) suffers from these problems: 1) because errors due to undershoots and overshoots posses large power, which make them overshadow errors from interest, and 2) because the presence of delays affects the RMSE severely, although it does not necessarily indicate poor performance, [66]. In this regard, the so-called filtered mean square error with delay correction, $\mathrm{FMSE_d}$, takes both phenomena into account, [66], as it first aligns estimated tremor with the

reference signal, and afterwards computes the delay corrected estimation error. The $\mathrm{FMSE_d}$ is defined as follows:

(25)

where ☐ represents and ☐ stands for the delay compensated tremor estimation. Instantaneous delay is calculated offline by means of an adaptive algorithm that minimizes the mean square error function based on a LMS-like recursion, [67]. As mentioned before, once instantaneous delay is obtained, RMSE between delay corrected estimation of tremor and the reference signal obtained is computed, providing the $\mathrm{FMSE_d}$.

First we select filter parameters so that they minimize $\mathrm{FMSE_d}$, and afterwards we compare the performance of each filter presented in Section 5.1.2. Optimal filters are:

- Weighted Frequency Fourier Linear Combiner with $\mu_0 = 5 \cdot 10^{-4}$, $\mu_1 = 2 \cdot 10^{-2}$, $\mu_b = 1 \cdot 10^{-2}$, $M = 1$, $f_0 = 6$ Hz.
- Bandlimited Multiple Fourier Linear Combiner with $\mu = 4 \cdot 10^{-2}$, $\mu_b = 0$, $M = 1$, $f_0 = 3$ Hz, $f_n = 8$ Hz, $G = 4$.
- Kalman Filter with $\mu_0 = 5 \cdot 10^{-4}$, $\mu_1 = 1 \cdot 10^{-2}$, $\mu_b = 1 \cdot 10^{-2}$, $M = 1$, $f_0 = 6$ Hz, $\mathbf{R} = 0.01$, $\mathbf{Q} = (1, 1, 1, 1)$.

Table VII summarizes FMSEd per task and patient for the optimal setup for the three algorithms. $\mathrm{FMSE_d}$ is computed as the error between applying the different tremor modelling algorithms to the estimated tremor, obtained as the difference between raw gyroscope signal and CDF estimation, and the zero phase offline estimation of tremor. We observe that among the WFLC, BMFLC, and KF, the KF (with a previous WFLC stage) performs the best when estimating instantaneous tremor amplitude, as it provides the least $\mathrm{FMSE_d}$ for all tasks, and also is capable of tracking tremor frequency in a robust fashion, as shown below. Therefore, we choose to employ a WFLC in cascade with a KF to estimate tremor parameters in real-time.

Algorithm	Arms outstretched	Finger to nose	Rest	Water into glass
Weighted Frequency FLC	0.017 ± 0.007	0.052 ± 0.023	0.014 ± 0.006	0.042 ± 0.020
Bandlimited Multiple FLC	0.007 ± 0.008	0.008 ± 0.019	0.005 ± 0.012	0.006 ± 0.013
Kalman Filter	0.001 ± 0.003	0.000 ± 0.002	0.001 ± 0.001	0.001 ± 0.003

Table VII. Filtered Mean Square Error with Delay correction (rad/s) for tremor estimation algorithms organized by task. Table provides mean ± standard deviation.

Figure 33 shows tremor amplitude and frequency estimation obtained with the WFLC alone, and together with the KF, during an arms outstretched task performed by patient 01. We observe that the WFLC is capable of adapting to tremor frequency and reacting when changes occur (bottom plot), and that KF adapts faster than WFLC when tremor amplitude varies. This happens because of the optimal nature of the KF, which makes it adjust its gain continuously, on the contrary to the WFLC that has a fixed gain to descent the gradient.

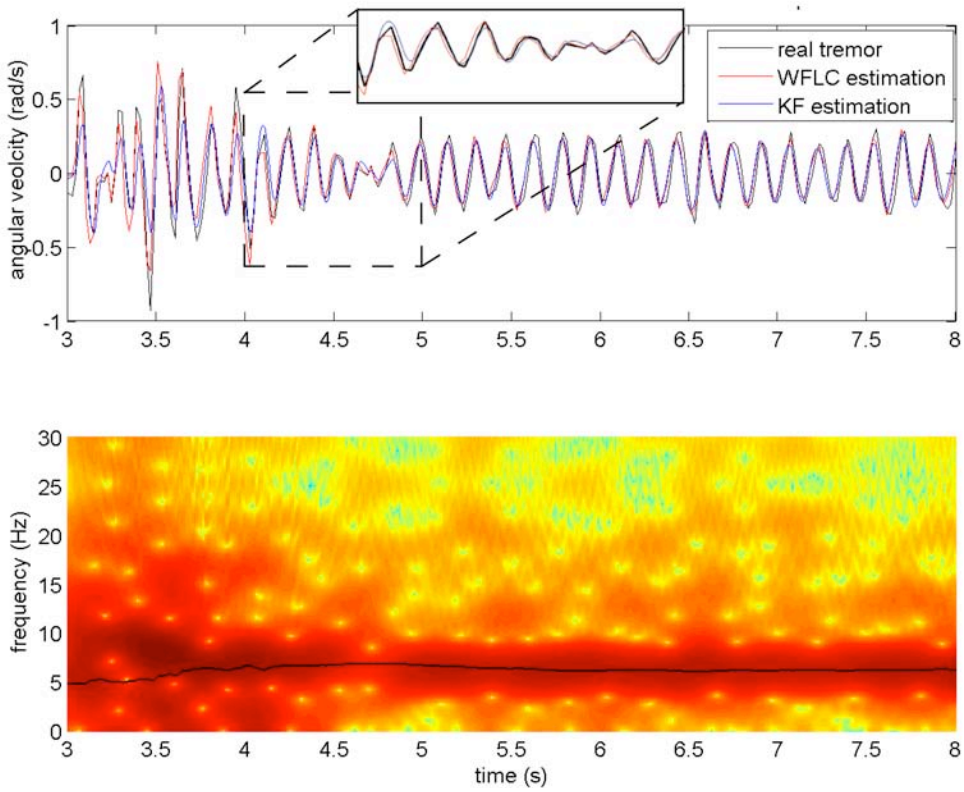

Figure 33. Top plot: Comparison between tremor amplitude tracking with the WFLC (blue line), and a cascade algorithm compound by a KF preceded by a WFLC (red line). Bottom plot: frequency tracking with the WFLC (solid line), plotted against tremor spectrogram. Data corresponds to an arms outstretched test performed by patient 01.

5.3. Discussion

Previous sections presented a two-stage algorithm for real-time estimation of tremor parameters. The first stage is in charge of separating voluntary and tremorous components of movement, based on the fact that tremor alters volitional motion in an additive manner, [53]. Next, we generate an estimation of tremor as the difference between raw motion and this estimated voluntary movement. The second stage estimates instantaneous tremor amplitude and frequency from isolated tremorous movement. We proposed and evaluated three algorithms for voluntary movement estimation, and three algorithms for tremor modelling.

Regarding voluntary movement estimation, we evaluated two g–h filters, the Benedict–Bordner (BBF) and Critically Dampened Filters (CDF), and a Kalman Filter (KF), for tracking volitional motion based on a figure of merit that accounts for tracking error and estimation smoothness, the Kinematic Tracking Error (KTE). This analysis yielded that g–h filters outperform the KF, because it results difficult to make it adapt quickly to changing voluntary movement patterns without tracking tremor, which translates into a larger KTE, Table VI. Comparing the performance of CDF and BBF, we observe that CDF outperforms BBF because its intrinsic oscillatory nature, that makes it resonate almost in phase with tremor. This occurs because the CDF has two equally spaced zeroes; thus it behaves as a critically dampened system, [59]. This also makes the CDF react faster when changes in volitional movement appear, decreasing estimation error during transitory periods. Therefore, the CDF constitutes the optimal filter during both steady and more dynamically complex tasks, as demonstrated by the fact that it provides the least KTE during both rest and finger to nose tests, Table VI.

Algorithms for estimation of instantaneous tremor frequency and amplitude are evaluated based on the Filtered Mean Square Error with Delay correction ($\mathrm{FMSE_d}$). This metric presents the advantages of accounting for errors due to undershoots and overshoots, and those originated from estimation delays, [66]. First, we evaluated two algorithms originally devoted to physiological tremor tracking, the Weighted Frequency Fourier Linear Combiner (WFLC), and the Bandlimited Multiple Fourier Linear Combiner (BMFLC). Physiological tremor not only has different aetiology than pathological tremors, but also manifests differently interms of amplitude and frequency, [46,48]. Although the WFLC has also been successfully employed in the context of pathological tremor

estimation, [50], we evaluated a novel approach based on a cascade algorithm compound by a WFLC and a Kalman Filter (KF). This algorithm raised as the best solution in the sense it minimizes the $\mathrm{FMSE_d}$, as it puts together accurate tremor frequency estimation based on a WFLC, and an independent KF for amplitude estimation, Table VII. In fact, its $\mathrm{FMSE_d}$ is at least five times smaller than that obtained with the BMFLC, which constitutes the second best candidate. KF tremor estimation proves to be robust and precise both during steady state regime and transitory periods, while the BMFLC and overall the WFLC lack of that accurate adaptation during transients, mainly because of the fixed gain they employ. This is demonstrated because performance in terms of FMSEd degrades the most during finger to nose and water glass tests, Table VII.

Therefore, the optimal architecture for the two-stage algorithm comprises a Critically Dampened Filter that estimates voluntary movement, and a cascade algorithm compound by a Weighted Frequency Fourier Linear Combiner that estimates tremor frequency and feds it into a Kalman Filter that tracks tremor amplitude, Figure 34. This approach provides an average tremor estimation error 0.001 ± 0.002 rad/s, with robust frequency tracking if compared to spectrograms.

Conclusions

This section presented a two stage algorithm for real-time estimation of instantaneous tremor parameters. At the first stage, the algorithm separates tremorous and concomitant voluntary movement based on their different distributions in the frequency domain. Next, estimated voluntary movement is removed from raw kinematic data, in order to generate an estimation of tremor. This estimation is then fed, at a second stage, into a Weighted Frequency Fourier Linear Combiner (WFLC) that tracks tremor frequency, and into a Kalman Filter that uses WFLC frequency information to estimate tremor amplitude. The resulting algorithm provides accurate estimation of tremor amplitude, with an average $\mathrm{FMSE_d}$ of 0.001 ± 0.002 rad/s, and robust frequency estimation when compared with spectrograms.

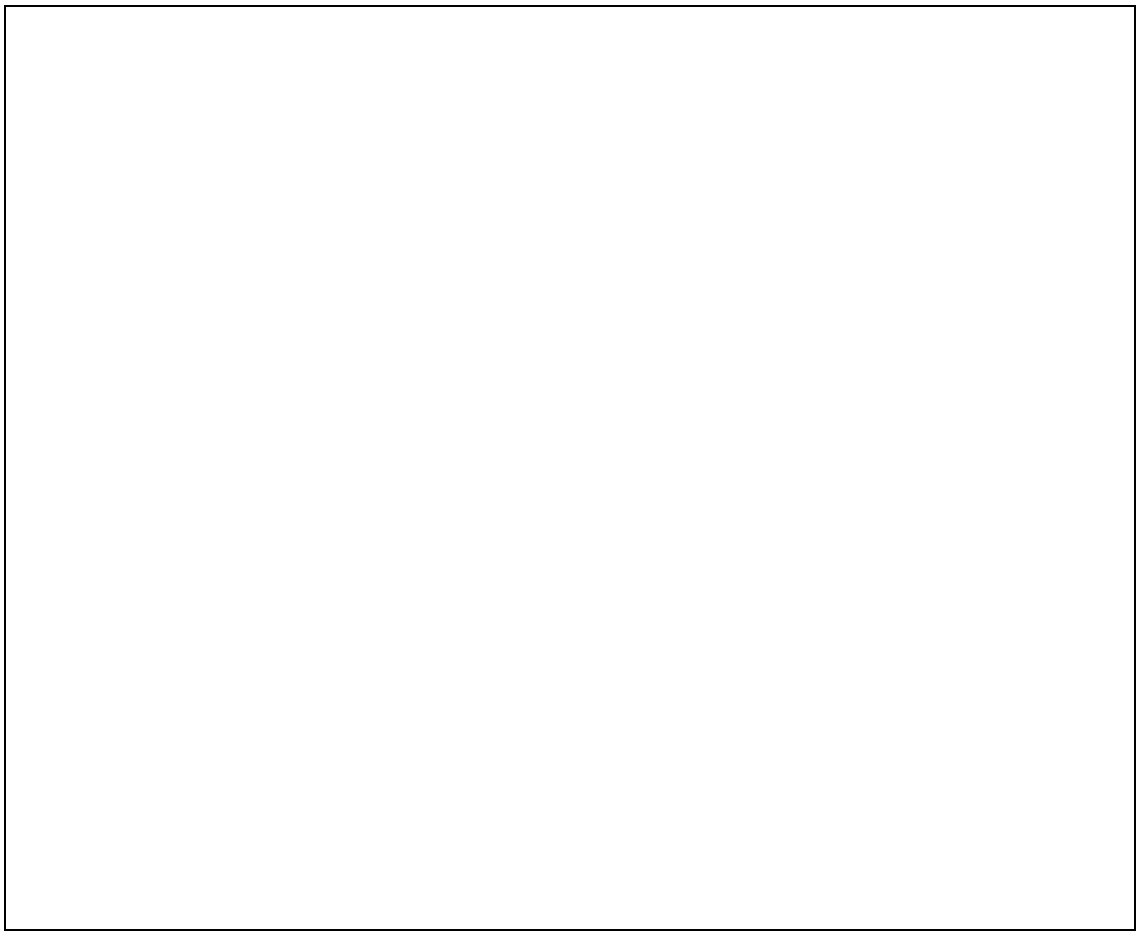

Figure 34: Block diagram summarizing the twostage algorithm for real-time estimation of instantaneous tremor parameters. First, a Critically Dampened Filter estimates voluntary motion from raw kinematic data. Next, we generate an estimation of tremor by subtracting voluntary from raw movement. At the second stage, the Weighted Frequency Fourier Linear Combiner estimates instantaneous tremor frequency, and then feds it into a Kalman Filter that tracks instantaneous tremor amplitude.

6. Algorithms for modality fusion

This section summarizes work on task WP4.5 *Algorithms for modality fusion*, which aims at integrating and/or fusing the information extracted from the different sensor modalities implemented in the TREMOR BNCI, to obtain a precise characterization of both voluntary and tremulous movements.

This task is coordinated by CSIC, and interacted with AAU, and URT for the integration of the different algorithms, and the identification of sensor fusion approaches. Notice that the work on this task will remain active, since the Consortium aims at taking advantage of the outcome of the different tasks in the TREMOR-EEU extension project, and the experimental sessions scheduled in the framework of these tasks, to improve the multimodal BCI part of the TREMOR system.

The work is organized as follows:

- Design and implement a hierarchical sensor integration scheme, to take advantage of the outcome of the different sensor modalities.
- Identify the sensor modalities which fusion may improve the performance and dependability of the multimodal BCI.
- Implement and validate off line, the sensor fusion scheme.
- Validate off line, with data from tremor patients, the sensor integration scheme.
- Implement the sensor integration scheme in the TREMOR platform.
- Include the sensor fusion algorithms in the integration scheme already implemented in the TREMOR platform.
- Validate in a experimental session with patients, the sensor integration scheme.

Notice that the four last tasks mentioned above remain still open, and will be finalised in the next recording sessions with tremor patients, which were reschedule in order to allow the definition of a new protocol that also address the work defined in TREMOR-EEU.

6.1 Hierarchical sensor integration scheme

The multimodal BCI information is merged following a hierarchical integration scheme, in which each sensor modality (that is aimed at extracting a certain piece of information, as described in previous sections) triggers the next one (in a descending sense), Figure 35.

First, a real–time EEG classifier is in charge of detecting user's intention to perform a voluntary movement, triggering the system. Next, processing of sEMG information yields tremor onset and an estimation of its frequency and phase. Finally, IMUs track instantaneous tremor amplitude and frequency at each joint. The use of multiple sensor modalities also permits us implementing fusion and redundancy techniques to enhance the dependability of the system, as it will be discussed below.

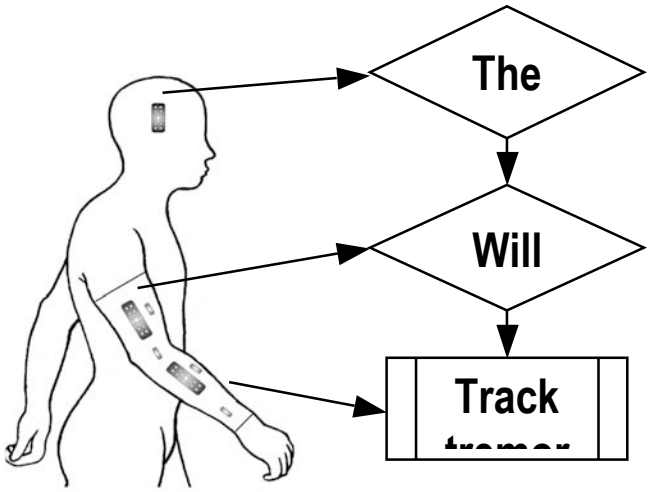

Figure 35. Integration scheme for the sensor modalities of the BNCI.

This approach serves both to optimize user's comfort and to minimize energy consumption, which is a critical aspect in all self-contained wearable devices. The benefits of the sensor fusion approach are two: 1) the patient will not be stimulated if tremor does not pose a functional issue, i.e. when there is no intention to perform a task, and 2) the patient is not stimulated in the absence of tremor, as tremor may not appear in certain patients during the execution of some tasks.

This hierarchical integration scheme also implements a redundancy mechanism by which the TREMOR system can be triggered by the estimation of voluntary movement form sEMG (see section 3) in case the EEG algorithm to detect movement intention suffers a false negative. This simple solution enhances greatly the dependability of the system, since detection of voluntary movement from sEMG is very precise.

6.2. Sensor fusion approach

The two major benefits from sensor fusion that we have identified are: 1) use of movement information to improve the performance of the EEG classifiers, enabling the implementation of a self-learning BCI, and 2) merge IMU and sEMG information to improve the performance of the tremor tracking algorithms, to tune the sEMG detection of tremor, and to compensate for delays on detection of tremor onset from sEMG information. The implementation of these ideas is detailed next.

Fusion of EEG and movement information

We have implemented a sensor fusion strategy for each movement intention classifier implemented:

1. Fusion of EEG and IMU modalities in the context of implementing learning mechanisms in the single trial EEG classifier (CSIC). The Bayesian EEG classifier, adjusts its parameters, namely feature gain, mean and covariance of the probabilistic density function, in real-time, based on voluntary movement detected with the inertial sensors, Figure 36.

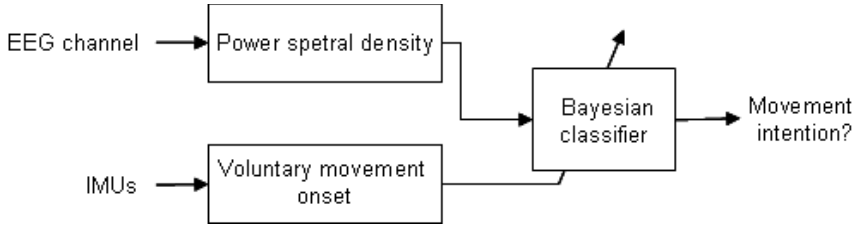

Figure 36. Fusion of EEG and IMU modalities in the Bayesian classifier. Detection of movement onset is employed to adjust the parameters of the ERD classifier.

2. Fusion of EEG and EMG modalities in the context of enhancing the robustness of ERD detection as an approach to detect movement intention (URT). This technique consists in recalculating, during the execution of the algorithm, the baseline associated with the no movement status, i.e. the reference with respect to which ERD is evaluated. This baseline is re-estimated in a dynamic window after movement offset as indicated by the deflection of EMG bursts, provided by Hodge's algorithm, [15]. This hybrid version of the classifier led to higher classification rates than the EEG-based version, including a higher specificity.

Fusion of sEMG and IMU information

As said above, fusion of sEMG and IMU information aims at compensating for delays in the detection of tremor, and improving the performance of the algorithm to extract tremor features.

1. Compensation of delays in tremor detection based on IMU recordings. Since the latency of the algorithm to detect tremor onset from sEMG is at least one tremor period, in some cases tremor may appear before the system receives the prediction (since the electromechanical delay can be less than a whole tremor period). Therefore, as the algorithm to calculate tremor features from the IMUs also estimates the voluntary component of the movement, we can use this as a redundancy mechanism to trigger the tremor suppression strategies.
2. Fusion of sEMG and IMU information to improve tremor frequency estimation. Although the performance of the two stage algorithm in frequency tracking is considerably accurate, the WFLC has a settling time of some seconds, which is highly correlated to the difference between the initial frequency guess and the actual tremor frequency. Hence, using the estimation of tremor frequency provided by the IHT algorithm

as initial guess, we can reduce drastically this interval, given the high precision of the IHT, and thus of the initial conditions for the frequency estimation algorithm.

7. Conclusions

This document describes the work carried under the framework of WP4 for the development of a multimodal BCI for real-time characterization of tremorous and concomitant voluntary movements to drive a tremor suppression neurorobot. This multimodal BNCI is implemented in a hierarchical approach, as described in the document, and implements the cognitive interaction (cHRI) between the user and the neurorobot developed in TREMOR.

Results shown demonstrate the ability of the cHRI to predict user's intention to perform a volitional movement, to detect the presence of tremor from sEMG, and to estimate its instantaneous amplitude and frequency out of kinematic information. Moreover, a number of features that will serve to enhance the reliability of the neurorobot were developed, for example: 1) taking advantage of the sEMG algorithm to estimate the onset of voluntary movement, to compensate for BCI based classification errors, 2) using the frequency estimation obtained by the IHT algorithm as an initial guess for the IMU based algorithm to track tremor features, 3) implementing machine learning techniques to adjust the parameters of the Bayesian classifier online, based on the execution of a voluntary movement.

This multimodal approach represents a step forward in BCI field. The novelty of our concept is:

- TREMOR concept tries to implement a self-training process through correlation of EEG-EMG. In our approach, the EEG baseline associated with the no movement status is updated online based on the information provided by EMG sensors.
- The algorithm to detect movement intention that we have develop, constitutes a step forward in BCI Systems, since: 1) it is an asynchronous online system, 2) it does not require subject training, and 3) it has been validated with patients with neurological conditions, i.e. different types of tremors.
- The multimodal BCI increases robustness of classical BCI systems through the use of redundant information at different stages of the neuromotor process: EEG (CNS), EMG (PNS) and IMU (biomechanics).
- The fusion of EEG and IMU modalities implemented learning mechanisms for the single trial EEG classifier. The Bayesian classifier resulted in an adaptive system that try to cope with the variability in EEG. This approach improves the performance of the asynchronous classifier, since compensates for the non-stationary characteristics of EEG phenomena.
- The fusion of EMG and IMU information provides precise characterization of both voluntary and tremolous movements in real time for every upper limb joint.
- TREMOR concept reduces computational burden as each modality is prone to provide different kinds of knowledge in a computationally inexpensive manner: EMG for tremor onset, EEG for intentionality of limb motion, IMUs for tremor amplitude and frequency. This allowed the implementation of a truly Real Time system.

According to Recommendation 3 of the First Annual Review meeting, which stated: "the project team is suggested to develop two prototypes in parallel. The first one would be the EEG-EMG-IMU based tremor compensation, as originally planned in the Description of Work, while the second one should be founded on EMG and IMU data only," the consortium has decided to implements a redundancy mechanism by which the TREMOR system can be triggered by the estimation of voluntary movement form sEMG. This was implemented for the platform that will be founded on EMG and IMU data.

Milestones M4.1.A, M4.1.B, M4.2.A, M4.2.B, M4.3, M4.4.A, M4.4.B, M4.5.A and M4.5.B have been met according to the results presented in this deliverable. Therefore, the BCI system has been optimized and implemented based on iterative process involving user trials. Notice that due to extension of the objectives of this WP in the framework of TREMOR-EEU extension, the work on this task will remain active, since the Consortium aims at improving the multimodal BCI part of the TREMOR system based on the results of TREMOR-EEU.

References

[1] D.M. Halliday, B.A. Conway, S.F. Farmer and J.R. Rosenberg, "Using electroencephalography to study functional coupling between cortical activity and electromyograms during voluntary contractions in humans", *Neurosci Lett*, 241, (1), 5-8, 1998.

[2] B.A. Conway, D.M. Halliday, S.F. Farmer, U. Shahani, P. Maas, A.I. Weir and J.R. Rosenberg, "Synchronization between motor cortex and spinal motoneuronal pool during the performance of a maintained motor task in man", *J Physiol*, 489 (Pt 3), 917-924, 1995.

[3] P. Brown, "Cortical drives to human muscle: the Piper and related rhythms", *Prog Neurobiol* , 60, (1), 97-108, 2000.

[4] B.A. Conway, S.F. Farmer, D.M. Halliday and J.R. Rosenberg, "On the relation between motor-unit discharge and physiological tremor", *Alpha and Gamma Motor Systems. Plenum Press*, New York, pp 596-598

[5] A.B. Vallbo and J. Wessberg, "Organization of motor output in slow finger movements in man", *J Physiol,* 469, 673-691, 1993.

[6] L. Faes, G.D. Pinna, A. Porta, R. Maestri and G. Nollo "Surrogate data analysis for assessing the significance of the coherence function", *IEEE Trans Biomed Eng*, 51, (7), 1156-1166, 2004.

[7] G.Severini, S.Conforto, M.Schmid, T. D'Alessio. Movement Intent as Predicted by Time-Varying Cortico-Muscular Coherence Estimated through MAR Models. *ICRA Workshop on Wearable Robots*, Kobe, Japan: May 12-17, 2009**.**

[8] G. Pfürtscheller, C. Brunner, A. Schlögl, and F. H. L. da Silva, "Mu rhythm (de)synchronization and EEG single-trial classification of different motor imagery tasks," *Neuroimage*, vol. 31, pp. 153–159, 2006.

[9] S. G. Mason and G. E. Birch, "A brain-controlled switch for asynchronous control applications," *IEEE Transactions on Biomedical Engineering*, vol. 47, no. 10, pp. 1297–1307, 2000.

[10] G. Townsend, B. Grainmann, and G. Pfürtscheller, "Continuous EEG classification during motor imagery-simulation of an asynchronous BCI", *IEEE Transactions on Neural Systems and Rehabilitation Engineering*, vol. 12, no. 2, pp. 258–265, 2004.

[11] G. Pfurtscheller, F.H. Lopes da Silva, "Event-related EEG/MEG synchronization and desynchronization: basic principles" Clin Neurophysiol, 110, (11), 1842-57, 1999.

[12] E. Brookner, "Tracking and Kalman Filtering Made Easy"; John Wiley & Sons: Hoboken, NJ, USA, 1998.

[13] G. Severini, S. Conforto, M, Schmid, T. D'Alessio. Development of a real-time algorithm for ERD/ERS detection for the discrimination between voluntary and un-voluntary activity. *TOBI*, Graz: 2-4 February, 2010

[14] G. Severini, S. Conforto, M, Schmid, C, De Marchis, T. D'Alessio. A Real-Time EEG-EMG multimodal approach for the detection of voluntary activity in patients affected by tremor impairment. *GNB*, Torino: 8-10 July, 2010

[15] P.W. Hodges and B.H. Bui, "A comparison of computer-based methods for the determination of onset of muscle contraction using electromyography", Electroencephalogr Clin Neurophysiol, 101, (6), 511-519,1996.

[16] Zhang D, Poignet P, Bo AP, Ang WT. Exploring peripheral mechanism of tremor on neuromusculoskeletal model: a general simulation study. IEEE Trans Biomed Eng, 2009;56(10):2359-2369.

[17] Fukumoto I. Computer simulation of Parkinsonian tremor. J Biomed Eng, 1986;8(1):49-55.

[18] Oguztoreli MN, Stein RB. The effects of multiple reflex pathways on the oscillations in neuro muscular systems. J Math Biol, 1976;3(1):87-101.

[19] Prochazka A, Gillard D, Bennett DJ. Implications of positive feedback in the control of movement. J Neurophysiol, 1997;77(6):3237-3251.

[20] Santillán M, Hernández-Pérez R, Delgado-Lezama R. A numeric study of the noise-induced tremor in a mathematical model of the stretch reflex. J Theor Biol, 2003;222(1):99-115.

[21] Stein RB, Oguztoreli MN. Tremor and other oscillations in neuromuscular systems. Biol Cybern, 1976;22(3):147-157.

[22] Dideriksen JL, Farina D.Gianfelici Multi-scale modeling of pathological tremor. XVIII ISEK Conf, Aalborg, Denmark, 2010.

[23] Dideriksen JL, Farina D. An integrative model of the surface EMG in pathological tremor. IEEE EMBS Conf, Buenos Aires, Argentina, 2010.

[24] Fuglevand AJ, Winter DA, Patla AE. Models of recruitment and rate coding organization in motor-unit pools. J Neurophysiol, 1993;70(6):2470-2488.

[25] Barry BK, Pascoe MA, Jesunathadas M, Enoka RM. Rate coding is compressed but variability is unaltered for motor units in a hand muscle of old adults. J Neurophysiol, 2007;97(5):3206-3218.

[26] Dideriksen JL, Farina D, Baekgaard M, Enoka RM. An integrative model of motor unit activity during sustained submaximal contractions. J Appl Physiol, 2010;108(6):1550-1562.

[27] Houk JC, Rymer WZ, Crago PE. Dependence of dynamic response of spindle receptors on muscle length and velocity. J Neurophysiol, 1981;46(1):143-166.

[28] Prochazka A, Gorassini M. Ensemble firing of muscle afferents recorded during normal locomotion in cats. J Physiol (Lond) 1998;507(1):293-304.

[29] Farina D, Mesin L, Martina S, Merletti R. A Surface EMG Generation Model with Multilayer Cylindrical Description of the Volume Conductor. IEEE Trans Biomed Eng, 2004;51(3):415-426.

[30] Keenan KG, Farina D, Merletti R, Enoka RM. Amplitude cancellation reduces the size of motor unit potentials averaged from the surface EMG. J Appl Physiol, 2006;100(6):1928-1937.

[31] Zajac FE. Muscle and tendon: properties, models, scaling, and application to biomechanics and motor control. Crit Rev Biomed Eng, 1989;17(4):359-411.

[32] Esteki A, Mansour JM. An experimentally based nonlinear viscoelastic model of joint passive moment. J Biomech, 1996;29(4):443-450.

[33] Marusiak J, Jaskólska A, Kisiel-Sajewicz K, Yue GH, Jaskólski A. EMG and MMG activities of agonist and antagonist muscles in Parkinson's disease patients during absolute submaximal load holding. J Electromyogr Kinesiol, 2009;19(5):903-914.

[34] Raethjen J, Lindemann M, Schmaljohann H, Wenzelburger R, Pfister G, Deuschl G. Multiple oscillators are causing parkinsonian and essential tremor. Mov Disord, 2000;15(1):84-94.

[35] Héroux ME, Pari G, Norman KE. The effect of inertial loading on wrist postural tremor in essential tremor. Clin Neurophysiol, 2009;120(5):1020-1029.

[36] Christakos CN, Erimaki S, Anagnostou E, Anastasopoulos D. Tremor-related motor unit firing in parkinson's disease: Implications for tremor genesis. J Physiol (Lond), 2009;587(20):4811-4827.

[37] Gianfelici F, Biagetti G, Crippa P, Turchetti C. Multicomponent AM-FM representations: An asymptotically exact approach. IEEE Trans Audio, Speech and Language Process, 2007;15(3):823-837.

[38] Huang NE, Shen Z, Long SR, Wu MC, Shih HH, Zheng Q, Yen NC, Tung CC, Liu HH. The empirical mode decomposition and the Hilbert spectrum for nonlinear and non-stationary time series analysis. Proc R Soc Lond. 1998;454(1971):903-995.

[39] Maragos P, Kaiser JF, Quatieri TF. On separating amplitude from frequency modulations using energy operators. In Proc IEEE Int Conf Acoust Speech Signal Process, ICASSP'92, 1992;2:1-4.

[40] Santhanam B, Maragos P. Multi-component AM-FM demodulation via periodicity-based algebraic separation and energy-based demodulation. IEEE Trans Commun, 2000;48(3):473-490.

[41] Dideriksen JL, Gianfelici F, Farina D. Detecting tremor from the surface EMG. ISEK 2010 Conf, Aalborg, Denmark, 16-19 June, 2010.

[42] Farina D, Cescon C, Merletti R. Influence of anatomical, physical, and detection-system parameters on surface EMG. Biol Cybern, 2002;86(6):445-456.

[43] Lawrence SM. Computing the discrete-time analytic signal via FFT. IEEE Trans Signal Process, 1999;47(9):2600--2603.

[44] Gallego JA, Rocon E, Pons JL. “Estimation of Instantaneous Tremor Parameters for FES–Based Tremor Suppression,” Proc IEEE/RAS International Conference on Robotics and Automation, 2010.

[45] Gallego JA, Rocon E, Roa JO, Moreno JC, Pons JL. “Real-time estimation of pathological tremor parameters from gyroscope data,” Sensors, 10: 2129-2149, 2010.

[46] Elble R. “Tremor: clinical features, pathophysiology, and treatment,” Neurologic Clinics 27: 679–695, 2009.

[47] Riviere CN, Rader RS, Thakor NV. "Adaptive canceling of physiological tremor for improved precision in microsurgery," IEEE Transactions on Biomedical Engineering, 45: 839–846, 1998.

[48] Veluvolu KC, Tan UX, Latt WT, Shee CY, Ang WT. "Bandlimited Multiple Fourier Linear Combiner for real-time tremor compensation," Proc International Conference of the IEEE Engineering in Medicine and Biology Society, 2007.

[49] Veluvolu KC, Latt WT, Ang WT. "Double adaptive bandlimited multiple Fourier Linear Combiner for real-time estimation/filtering of physiological tremor," Biomedical Signal Processing and Control, 5: 37–44, 2010.

[50] Rocon E, Belda-Lois JM, Ruiz AF, Manto M, Moreno JC, Pons JL. "Design and validation of a rehabilitation robotic exoskeleton for tremor assessment and suppression," IEEE Transactions on Neural Systems and Rehabilitation Engineering, 15: 367–378, 2007.

[51] Bó APL, Poignet P, Geny C. "Filtering voluntary motion for pathological tremor compensation,"Proc IEEE/RSJ International Conference on Intelligent Robots and Systems, 2009.

[52] Tong K, Granat MH. "A practical gait analysis system using gyroscopes," Medical Engineering and Physics, 21: 87–94, 2009.

[53] Riley PO, Rosen MJ. "Evaluating manual control devices for those with tremor disability," Journal of Rehabilitation Research and Development, 24: 99–110, 1987.

[54] Riviere CN. "Adaptive Suppression of Tremor for Improved Human Machine Control," PhD Thesis; John Hopkins University: Baltimore, MD, USA, 1981.

[55] Mann KA, Werner FW, Palmer AK. "Frequency spectrum analysis of wrist motion for activities of daily living," Journal of Orthopaedic Research, 7: 304–306, 1989.

[56] Deuschl G, Raethjen J, Lindemann M, Krack P. "The pathophysiology of tremor," Muscle & Nerve, 24: 716–735, 2001.

[57] Grimaldi, G.; Manto, M. Tremor: from Pathogenesis to Treatment, Morgan & Claypool: San Rafael, CA, USA, 2008.

[58] Widrow B, Glover JR, McCool JM, Kaunitz J, Williams CS, Hearn RH, Zeidler JR, Dong E, Goodlin RC. "Adaptive noise canceling: Principles and applications," Proceedings of the IEEE 63: 1692–1716, 1975.

[59] Brookner, E. Tracking and Kalman Filtering Made Easy, John Wiley & Sons: Hoboken, NJ, USA, 1998.

[60] Benedict TR, Bordner GW. "Synthesis of an optimal track-while-scan smoothing equations," IRE Transactions on Automatic Control, 7: 27–32, 1962.

[61] Bar-Shalom Y, Li XR. Estimation and Tracking: Principles, Techniques and Software; Artech House Publishers: Norwood, MA, USA, 1998.

[62] O'Suilleabhain PE, Matsumoto JY. "Time-frequency analysis of tremors," Brain 121: 2127–2134, 1998.

[63] Vaz C, Kong X, Thakor N. "An adaptive estimation of periodic signals using a Fourier linear combiner," IEEE Transactions on Signal Processing, 42: 1–10, 1994.

[64] Rocon, E. "Reducción Activa de Temblor Patológico de Miembro Superior Mediante Exoesqueletos Robóticos," PhD Thesis; Universidad Politécnica de Madrid: Madrid, Spain, 2006.

[65] Kotovsky J, Rosen MJ. "A wearable tremor-suppression orthosis," Journal of Rehabilitation Research and Development, 35: 373–387, 1998.

[66] Gonzalez JG, Heredia EA, Rahman T, Barner KE, Arce GR. "Optimal digital filtering for tremor suppression," IEEE Transactions on Biomedical Engineering, 47: 664–673, 2000.

[67] Etter D, Stearns S. "Adaptive estimation of time delays in sampled data systems," IEEE Transactions on Acoustics, Speech Signal Processing, 29: 582–587, 1981.

[68] Pons JL, "Wearable Robots: Wearable robots: biomechatronic exoskeletons", Wiley, 2008.

[69] Deecke Lüder and Kornhuber Hans Helmut, "Changes in the brain potential in voluntary movements and passive movements in man: readiness potential and reafferent potentials". Pflüger Arch., Vol. 284, 1-17, 1965.

[70] Morash Valerie, "Classifying EEG signals preceding right hand, left hand, tongue, and right foot movements and motor imageries", Clinical Neurophysiology, Vol. 119, 2570-2578, 2008.

[71] Salenius Stephan, “Cortical Control of Human Motoneuron Firing During Isometric Contraction”, The American Physiological Society, Vol. 97, 3401-3405, 1997.

[72] Noordhout Alain Martens de [et al.], “Corticomotoneuronal synaptic connections in normal man. An electrophysiological study”, Brain, VOL. 122, 1327-1340, 1999.

[73] Bai Ou et al., “Prediction of human voluntary movement before it occurs”, Clinical Neurophysiology, 2010.

[74] Buzsáki György, “Rhythms of the Brain”, Oxford University Press, 2006.

[75] Popescu Florin et al., “Single Trial Classification of Motor Imagination Using 6 Dry EEG electrodes”, PLoS ONE, 2007.

[76] Shibasaki Hiroshi and Hallett Mark, “What is the Bereitschaftspotential?”, Clinical Neurophysiology, Vol. 117, 2341-2356, 2006.

Annex 1. Estimation of cortico-muscular coherence (CMC) between EEG and EMG signals.

Magnitude Squared Coherence (MSC) is a parameter used to assess the linear association between two signals in the frequency domain. It is expressed as the ratio between the cross spectrum of the two signals and the product of their auto spectra (see the MSC equation provided below).

$$\left|C_{12}(f)\right|^2 = \frac{\left|P_{12}(f)\right|^2}{(P_{11}(f) \cdot P_{22}(f))}$$

Cortico-muscular coherence (CMC) is an instance of MSC, when the two signal components are cortical EEG signal and rectified sEMG. Thus it represents a measure of coupling between the cortical activity as recorded from EEG in the cortical area and the muscular activity as extracted from rectifying the sEMG signal of a given muscle, [1]. Many studies in literature indicate that CMC contributions in the beta band (15-30 Hz) are related to the preparation of voluntary activity during sub-maximal contractions, [2], and represent the index of synchronization of motor units discharge at different frequencies, as elicited by the descending drives, [3]. Moreover, CMC contributions in the 5-12 Hz band have been associated to drives of physiological tremor, [4-5]. By monitoring over time the evolution of CMC in these two specific bandwidths it is possible to estimate the onset of voluntary activity and tremor, respectively.

In order to timely estimate CMC, a method based on a bivariate auto-regressive (BAR) representation of the signals under analysis has been implemented in the framework of WP 4.1. Parameters of the BAR model are have been used to characterize a closed-loop representation of the generation of the two signals and to represent the evolution over time of CMC. The estimation underwent a thresholding procedure based on the significance assessment of CMC values: values below the estimated threshold were zeroed. The threshold estimation is based on the surrogate data analysis presented in [6]. When significant coherence values in the beta band appear for at least 200 ms, the beginning of voluntary activity is revealed, [7]. The same procedure can be applied in the 5-12 Hz band for the detection of tremor.

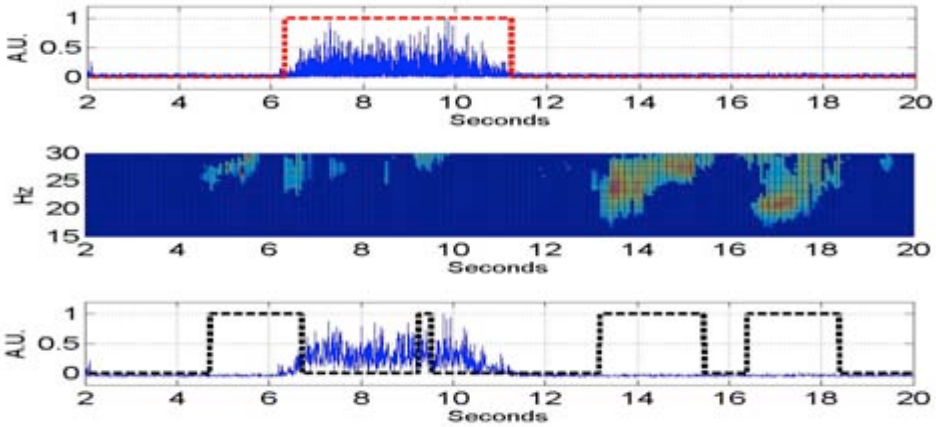

Figure A. Top plot represents EMG with muscular activation as reference (red); middle plot represents CMC map; bottom plot represents EMG with output of the algorithm (black).

Results obtained using this method showed significant contribution of CMC in the beta band around 1 second before the beginning of the voluntary movements in single wrist movement tasks. Nevertheless, the algorithm reveals beta band CMC contributions after the end of the movement, possibly associated with resynchronization of cortical activity. While this method is able to timely reveal when dealing with simple wrist movements, it is here to be outlined that the computational cost for surrogate data analysis limits the real-time implementation of the method.

Annex 2. Analysis of different factors in the BCI prediction of voluntary movement.

In order to evaluate possible relationships between the different pathologies causing tremor and the ERD features, an analysis of variance (ANOVA) has been performed on the data of all the experimental sessions carried out during the Tremor project involving EEG measurements while subjects performed self-paced movements of the dominant arm. The total dataset and the four factors considered are listed in Table A.

		N
Gender	F	5
	M	15
Age_Range	20-40	7
	40-65	4
	65-90	9
Diagnosis	C	6
	ESVO	1
	ET	8
	MT	1
	PD	3
	PTT	1
Condition	C	6
	P	14

Table A. Inter-subjects factors. Diagnosis code: Control (C), Extrapyramidal Syndrome of Vascular Origin (ESVO), Essential Tremor (ET), Mixed Tremor (MT), Parkinson's disease (PD), Post-traumatic Tremor (PTT). Condition code: Control (C), Patient (P).

The dependent variables extracted for each subject measured were:

- *ERD anticipation.* The length of the interval from the time at which the average ERD shows a significant decrease to the movement onset).
- *Power decrease.* Ratio between the movement state power spectrum and the basal state power spectrum at the frequency where the highest difference is found.
- *Frequency of the alpha rhythm*.

Results

No statistically significant differences of the ERD characteristics were found between the control and patient groups as well as within the different tremor groups (different pathologies). Although it has been demonstrated that the ERD features in patients with Parkinson's disease change with respect to healthy subjects, [77, 78], the data collected and used in this study did not show any such differences. This might be due to the lack of a sample dataset representative enough for each one of the groups considered.

Only a significant difference between the power decrease of the patient groups above and below 65 years old was found ($F=8.686$, $p=0.016$, $\alpha = 0.05$) (Table B). These results were expected a priori since the influence of the age on the sensorimotor rhythms desynchronization is well documented in the literature, [79].

(I)Age_Range	(J)Age_Range	Means Differences (I-J)	Typical error	Sig.	Confidence Interval 95%	
					LowerLimit	Upper Limit
20-40	40-65	-4,4643	5,66710	,719	-20,2869	11,3583
	65-90	11,5079	4,55652	,076	-1,2139	24,2298
40-65	20-40	4,4643	5,66710	,719	-11,3583	20,2869
	65-90	15,9722*	5,43331	,040	,8024	31,1420
65-90	20-40	-11,5079	4,55652	,076	-24,2298	1,2139
	40-65	-15,9722*	5,43331	,040	-31,1420	-,8024

Table B. Multiple Comparisons for the ERD power decrease factor. Mean quadratic error = 81,750. *. α = 0,05.

References

[77] Magnani G, Cursi M, Leocani L, Volonté MA, Locatelli T, Elia A, et al. Event-related desynchronization to contingent negative variation and self-paced movement paradigms in Parkinson's disease. Movement disorders: official journal of the Movement Disorder Society. 1998 Jul;13(4):653-60.

[78] Lim VK, Hamm JP, Byblow WD, Kirk IJ. Decreased desychronisation during self-paced movements in frequency bands involving sensorimotor integration and motor functioning in Parkinson's disease. Brain Research bulletin. 2006 Dec;71(1-3):245-51.

[79] Derambure P, Defebvre L, Dujardin K, Bourriez JL, Jacquesson JM, Destee a, et al. Effect of aging on the spatio-temporal pattern of event-related desynchronization during a voluntary movement. Electroencephalography and clinical neurophysiology [Internet]. 1993 Jun;89(3):197-203. Available from: http://www.ncbi.nlm.nih.gov/pubmed/7686852.